Boone Samuel C (Orcid ID: 0000-0003-2274-7933)
Kohn Barry P. (Orcid ID: 0000-0001-5064-5454)
Gleadow Andrew J.W. (Orcid ID: 0000-0003-0496-0028)
Foster David (Orcid ID: 0000-0002-5603-9372)

Influence of rift superposition on lithospheric response to East African Rift System extension: Lapur Range, Turkana, Kenya

Samuel C. Boone[1], Christian Seiler[1], Barry P. Kohn[1], Andrew J. W. Gleadow[1], David A. Foster[2] and Ling Chung[1]

[1]School of Earth Sciences, University of Melbourne, VIC 3010, Australia

[2]Department of Geological Sciences, University of Florida, Gainesville, FL, 32611, U.S.A.

Corresponding author: Samuel C. Boone (sboone@student.unimelb.edu.au)
†School of Earth Sciences, University of Melbourne, 3010, VIC, Australia

Key Points:

- Data and modelling show Early Cretaceous (between 100-120 Ma) and rapid middle Miocene-Recent cooling episodes
- Latter period of cooling marks middle Miocene onset of East African Rift System (EARS) extension in northern Turkana Basin
- Low effective elastic thickness and high heat flow of Turkana lithosphere amplified isostatic footwall uplift in response to EARS extension

This is the author manuscript accepted for publication and has undergone full peer review but has not been through the copyediting, typesetting, pagination and proofreading process, which may lead to differences between this version and the Version of Record. Please cite this article as doi: 10.1002/2017TC004575

Abstract

The Turkana Depression of northern Kenya, lies at the intersection of the NW-SE trending late Mesozoic-early Paleogene South Sudan and Anza rifts and the N-S trending late Paleogene-Recent East African Rift System (EARS). A low-temperature thermochronology study in the Lapur Range reveals a complex tectonothermal evolution related to multiple periods of regional and local tectonism. Zircon (U-Th)/He data from Precambrian basement record rapid Early Cretaceous denudational cooling. Coeval subsidence in the adjacent Anza and South Sudan rifts suggests that the northern Turkana region acted as a basement high separating the grabens, as well as an axial source of sediment. Between ~95-90 Ma, a period of reheating commenced with burial of Lapur basement beneath ~500 m of Turonian-Eocene Lapur Sandstone and ~1.5-3.5 km of latest Eocene-early Miocene Turkana Volcanics. Apatite fission track (AFT) and apatite (U-Th-Sm)/He data record a transition to rapid denudational cooling in the mid Miocene (~14 Ma) in response to EARS-related extension in the northern Turkana Basin. Thermal history models indicate the Lapur Range experienced ~90-100 °C of mid-Miocene to Plio-Pleistocene cooling, yielding the first Neogene AFT ages reported from Kenya related to EARS exhumation. We attribute the larger magnitude of cooling in the Lapur Range compared to other regions of the EARS to the attenuated crustal thickness and elevated heat flow of the Turkana Depression, crustal properties inherited from earlier Cretaceous-Paleogene rifting. The resulting low effective elastic thickness of the Turkana lithosphere allowed for increased isostatic footwall uplift in response to EARS extension.

1 Introduction

The East African Rift System (EARS) is the foremost modern example of a continental rift zone on Earth and has been pivotal in developing our understanding of the early stages of rifting and continental breakup. Extending ~3,500 km from the Red Sea coast of northern Ethiopia to Mozambique, the EARS is considered to be an intra-cratonic prelude to oceanic opening (Chorowicz, 2005; Morley, Ngenoh, & Ego, 1999) (Figure 1). Rifting in the EARS is localized within two extensive regions of crustal uplift, the northern Ethiopian Dome and the southern East African Dome, averaging 1,500 and 1,200 m elevation respectively. These two plateaux are separated by the Turkana Depression, a broad region of relatively subdued topography (average ~600 m) running NW-SE from the plains of South Sudan, through southern Ethiopia and northern Kenya, to the Kenyan coast. Here, at the junction of the Ethiopian and Kenyan Rifts, the Turkana Depression displays a complex history of rifting, rift-sedimentation and crustal thinning that is in stark contrast to the rest of the EARS.

Evolution of the Turkana Depression commenced at least as far back as the Late Jurassic during a regional extensional phase that resulted in the development of the large NW-SE trending South Sudan and Anza Rifts, the latter of which is traditionally thought to extend from the Kenyan coast to the eastern shores of Lake Turkana (Figure 1) (Ebinger et al., 2000; Morley, Bosworth, et al., 1999; Schull, 1988). A proposed subsurface link between these late Mesozoic-Paleogene rifts is believed to lie near the Kenyan-Ethiopian border, west

of Lake Turkana (Bosworth, 1992; Ebinger, Yemane, Woldegabriel, Aronson, & Walter, 1993; Ibrahim, Ebinger, & Fairhead, 1991). During the Paleogene, a series of extensional basins developed in the Turkana region as part of a larger, poorly understood NNW-SSE rifting trend stretching from Sudan, along the South Sudanese-Ethiopian border and down into eastern Kenya (Bosworth, 1992; Hendrie, Kusznir, Morley, & Ebinger, 1994). Oligocene?- Miocene to Recent EARS rifting was superimposed again, forming approximately N-S trending basins sub-parallel to those of the neighbouring Ethiopian and Kenyan Rifts, reactivating some pre-existing structures and abandoning others (Hendrie et al., 1994; Morley, Stone, Harper, & Wigger, 1999). Consequently, compared to the Ethiopian and Kenyan Rifts, the present-day Turkana segment exhibits anomalously thin crust (~20 km) and elevated heat flow (Benoit et al., 2006; Sippel et al. 2017).

Despite over a century of work investigating continental rifting in East Africa, significant uncertainty remains concerning the spatiotemporal evolution of extension in the long-lived Turkana portion of the EARS. This is largely due to poor surface exposure of older rift deposits in Turkana, which are often buried beneath thick volcanic sequences or by Lake Turkana itself (Morley, Stone, et al., 1999).

Low-temperature thermochronology, such as apatite fission track (AFT), apatite (U-Th-Sm)/He (AHe) and zircon (U-Th)/He (ZHe) analyses, together with thermal history modelling provide a powerful approach to investigate the tectono-thermal evolution of the uppermost ~10 km of the crust. These methods have often been utilized in rift settings to constrain footwall exhumation histories and the propagation of extension over time (e.g. Brown et al., 1990; Sullivan et al., 2000; Lisker et al., 2003; Seiler et al., 2011; Feinstein et al., 2013). Although several low-temperature thermochronology studies have previously investigated the timing and magnitude of faulting in other parts of the EARS (e.g. Foster and Gleadow, 1992, 1993, 1996; Wagner et al., 1992; Noble et al., 1997; Spiegel et al., 2007; Pik et al., 2008; Bauer et al., 2012, 2013; Torres Acosta et al., 2015), very few data are available from the Turkana Depression. A more precise understanding of the thermal evolution of the Turkana crust may reveal clues about how rifting has propagated over time in Turkana and how its lithospheric response to extension has been affected by multi-phase rift superposition.

Here, we present AFT, AHe and ZHe data for 10 samples from basement and overlying sedimentary rocks collected from the Lapur Range escarpment and along the ~E-W Lokitaung Gorge that incises the range. The Lapur Range is an exposed basement block in the footwall of the ~N-S Murua Rith-Lapur (MRL) master fault that bounds the northern Turkana Basin. Its location precisely at the intersection of the Cretaceous-early Paleogene Anza-South Sudan Rifts and the Neogene-Recent EARS presents a unique opportunity to investigate the effects of rift superposition on the region's upper crustal thermal evolution. Combined thermal history modelling reveals a comprehensive late Mesozoic-Recent tectono-thermal evolution of the Lapur block, providing important spatiotemporal constraints on the propagation of rifting in the Turkana Depression.

1.1 Tectonic and Geological Setting

Africa has been a centre of continental accretion since the late Proterozoic, with its modern terrane configuration having been established during the late Neoproterozoic-Early

Paleozoic Pan-African Orogeny. The tectonic, magmatic and metamorphic activity of the Pan-African Orogeny culminated in the amalgamation of the supercontinent Gondwana (Kröner & Stern, 2005). The related ocean closure, arc and microcontinent accretion and the suturing of continental fragments resulted in a series of orogenic and mobile belts throughout Gondwana, including the Mozambique Belt that runs through modern-day Kenya and consists of Neoproterozoic passive margin sediments intercalated with Archean gneisses (Begg et al., 2009).

The early Paleozoic was marked by pervasive postorogenic magmatism, shearing, major tectonic uplift and deep seated exhumation of mobile belts throughout Gondwana (Unrug, 1997). Breakup of Gondwana began in earnest during late Paleozoic-Jurassic Karoo rifting as evidenced by the formation of widespread intracratonic rift basins over much of southern and eastern Africa (Kreuser, 1995).

1.1.1 Jurassic-Paleogene Anza and South Sudan Rifts

The NW-SE trending Anza Rift encompasses an area of extended continental crust stretching ~600 km from the Kenyan coast to the eastern shores of Lake Turkana (Figure 1) (Reeves, Karanja, & MacLeod, 1987). The eastern portion of the trough, in the Lamu Embayment area, is thought to have initially formed as an aulacogen during the break-up of Madagascar from East Africa in the Early-Middle Jurassic (Greene, Richards, & Johnson, 1991) and was later reactivated during Cretaceous-Paleogene rifting. The sedimentary record of the Anza Rift is dominated by Upper Cretaceous-Paleogene lacustrine shales and fluvio-deltaic sandstones, showing an overall trend of younger rift activity towards the southeast (Morley, Bosworth, et al., 1999). Unlike later EARS rifting, Cretaceous-Paleogene extension was not accompanied by significant igneous activity (Morley, Ngenoh, et al., 1999).

The Cretaceous-Paleogene Abu Gabra, Muglad and Bahr el Arab rifts, collectively known as the South Sudan Rifts (Figure 1), formed in relation to the opening of the South and Equatorial Atlantic (Guiraud & Maurin, 1992). In the southeast the basins narrow towards the South Sudanese-Kenyan border, however due to a data gap in eastern South Sudan and superposition of later Paleogene-Recent EARS rifting in northern Kenya, the geometry of this termination remains uncertain (Guiraud & Bosworth, 1997). The compatible architecture, coeval timing and similar gravity signal suggest that the Anza Rift may be linked to the South Sudan Rifts in northern Turkana (Ibrahim et al., 1991; Schull, 1988). A half-graben basin of possible Cretaceous-Paleogene age detected by seismic imaging beneath the Lotikipi Plains of western Turkana (Figure 2) (Wescott, Wigger, Stone, & Morley, 1999) and the presence of Upper Cretaceous sediment elsewhere in Turkana suggests the Anza and South Sudan Rifts could be linked via a series of smaller rift basins that have since been masked by Neogene rifting in northern Kenya. Alternatively, the two rift systems may be connected via the proposed dextral South Sudan Shear Zone (Figure 1) (e.g. Browne and Fairhead, 1983; Bosworth, 1992).

1.1.2 Paleogene-Recent East African Rift System (EARS)

The EARS comprises two rifts trends, an eastern and western branch, manifested in two narrow (50-150 km) corridors of asymmetric half-grabens developed above listric faults with rollover anticlines in the hanging wall, which follow a trend of Precambrian mobile belts (Figure 1) (Morley, Ngenoh, et al., 1999). In general, volcanism in the EARS started earlier than extension, with the earliest manifestation being tholeiitic flood basalts emplaced between 45 and 33 Ma in the northern Turkana Depression (Bellieni et al., 1981; Ebinger et al., 1993; R. M. George & Rogers, 2002; Wescott et al., 1999). The volcanically-rich eastern branch consists of the Ethiopian and Kenyan Rifts, where EARS-related extension began in the early Miocene (Morley, Ngenoh, et al., 1999). However, there is some evidence for earlier rift activity in the Turkana Depression during the Paleogene (Bosworth & Morley, 1994; Ebinger et al., 1993; Hendrie et al., 1994; Morley, Stone, et al., 1999; Wescott et al., 1999).

1.1.3 Turkana Depression

The pattern of rifting in the Turkana Depression contrasts with the rest of East Africa in terms of both duration and deformation style (Figure 2). Anza rifting likely commenced in the Early Cretaceous on the east side of Lake Turkana, but by Paleogene time extensional tectonics had migrated to the west where it linked up with the South Sudan rifts (Bosworth, 1992; Hendrie et al., 1994; Wescott et al., 1999). EARS-related rifting began in western the Turkana Depression by the late Oligocene and migrated eastward during the Miocene, initiating the rift basins underlying Lake Turkana and their onshore equivalents by the late Miocene (Baker & Wohlenberg, 1971; Morley, Stone, et al., 1999). During the latest Pliocene-Pleistocene (< 3 Ma), extension in the Turkana Depression localised into a narrower zone of igneous intrusions and minor faults east of Lake Turkana, in alignment with coevally developed dike and fault swarms observed in the Ethiopian and Kenyan rifts (Morley, Ngenoh, et al., 1999). As a result, the modern Turkana Depression consists of a series of N-S striking half-grabens that are bound by steep (~65°) east-dipping listric normal faults, which are thought to sole into a shallow crustal ductile detachment at ~10-12 km depth (Morley, Stone, et al., 1999). These master faults have several kilometres of vertical throw, providing the accommodation space for up to ~7 km of late Cenozoic sediments (Chorowicz, 2005). The Lokichar Basin (Figure 2) alone experienced over 10 km of extension (Morley et al., 1992).

The prolonged duration of rifting, superposition of multiple rift phases and longitudinal propagation of extension resulted in the Turkana Depression being the widest part of the EARS (~150 km, consisting of 3-4 major half-grabens) (Morley, Stone, et al., 1999), as well as the area of thinnest continental crust south of the Afar (18-20 km under western Turkana, compared to 35-40 km under the Kenyan Rift) (Henry et al., 1990; Maguire, Swain, Masotti, & Khan, 1994; Mechie et al., 1994).

1.1.4 Lapur Range

The Lapur Range, attaining elevations of up to 1560 m a. s. l., is located along the northwest shores of Lake Turkana at the intersection of the failed Anza-South Sudan Rifts

(Figure 3). The Lapur block sits in the footwall of the MRL Fault, a N-S trending, east-dipping normal fault that bounds the western side of the northern Turkana Basin (Figure 4a) (Abdelfettah et al., 2016; Morley et al., 1992; Tiercelin et al., 2012). The northern Turkana Basin is a generally N-S trending, westward-dipping half graben that hosts present-day Lake Turkana. Based on seismic interpretations, it is thought to have begun to form in the middle Miocene (15-10 Ma) (Dunkelman, Rosendahl, & Karson, 1989; Morley et al., 1992; Morley, Stone, et al., 1999).

The basement of the Lapur Range is composed of Precambrian Mozambique Belt gneisses, amphibolites, granulites and other metamorphic assemblages (Begg et al., 2009). The basement is overlain by the Upper Cretaceous-lower Paleogene Lapur Sandstone (Arambourg & Wolff, 1969), which is up to 500 m thick and thinning to the north and south. The unconformity and bedding in the Lapur Sandstone dip ~15° to the WSW to SW, as dip direction varies slightly throughout the range (Morley et al., 1992; Tiercelin et al., 2012). Rocks exposed in the NE Lapur block therefore represent structurally deeper crustal levels than those in the south and west of the range. The Lapur Sandstone is interpreted as a fluvial deposit that was axially fed into the Anza Rift (Morley et al., 1992), with the lowest strata estimated as Turonian-early Campanian based on the presence of dinosaur and reptilian fossils (O'Connor, Sertich, & Manthi, 2011). The uppermost beds are locally interbedded with basal flows of the overlying Turkana Volcanics (Tiercelin et al., 2012).

The Turkana Volcanics were emplaced between ~37-17 Ma and consist of upper Eocene-Oligocene basalts and interbedded tuffs, overlain by lower-middle Miocene rhyolites (Morley et al., 1992; Walsh & Dodson, 1969; Zanettin, Justin Visentin, Bellieni, Piccirillo, & Francesca, 1983). The total thickness of volcanics varies between basins to the west and east of the Lapur Range, ranging from ~3650 m in the Gatome Basin to ~1250 m under northern Lake Turkana, respectively (Morley et al., 1992; Wescott et al., 1999).

The subsurface stratigraphy in the hanging wall of the MRL Fault is primarily known from an ~E-W trending onshore seismic line (TVK-10; Figures 3 & 4a). Wescott et al. (1999) interpreted the seismic data as showing the Middle Miocene Turkana Volcanics conformably overlain by a thick pile (up to 2 s TWTT) of late Miocene-Pliocene sedimentary rocks. Due to the highly degraded quality of seismic data below the Turkana Volcanics, the deeper basin structure is almost entirely unknown (Wescott et al., 1999). However, a recent reinterpretation of the same seismic line identified a ca. 300 m thick sedimentary package in the MRL hanging wall underlying the Turkana Volcanics, which was interpreted as a continuation of the Lapur Sandstone (Tiercelin et al., 2012). Only the uppermost portion of the basin fill crops out and comprises the Plio-Pleistocene Nachukui Formation, fluvio-lacustrine sediments dated between 4.2 and 0.7 Ma (Feibel, Brown, & McDougall, 1989). Offshore seismic data from Lake Turkana indicate a 4-km thick sedimentary package overlying the Turkana Volcanics (Dunkelman et al., 1989).

1.1.5 Previous low-temperature thermochronology studies

Previous thermochronological studies in East Africa are primarily based on AFT and show that the regional basement underwent early Mesozoic monotonic cooling related to craton exhumation. The oldest AFT ages (>250 Ma) are reported from the Tanzanian Craton

in SW Kenya (Charles H. Kasanzu, 2016; Charles Happe Kasanzu et al., 2016; M Wagner et al., 1992). In some places however, this pattern has been disrupted by Cretaceous and Paleogene episodes of rapid cooling associated with rift-related denudation. Cretaceous to Paleogene cooling events are recorded in several locations throughout Kenya, including the Karisia Hills (>120 and 70-50 Ma; Foster and Gleadow, 1992), the Cherangani Hills (~70-50 Ma; Foster and Gleadow 1993, 1996) as well as the Samburu Hills and Elgeyo Escarpment (~50-35 Ma; Torres Acosta et al., 2015) (Figure 2). Similar ages are found in neighbouring Tanzania (W P Noble et al., 1997) and Ethiopia (Balestrieri, Bonini, Corti, Sani, & Philippon, 2016; Philippon et al., 2014). This pervasive Cretaceous-Paleogene phase of rapid cooling has been interpreted as resulting from denudation of the Anza rift shoulders during the graben's formation (Foster & Gleadow, 1992).

To date, Neogene cooling in Kenya related to EARS faulting and footwall erosion has only been inferred from thermal history modelling of low-temperature thermochronology data from the base of the Kenyan Rift flanks (Spiegel et al., 2007; Torres Acosta et al., 2015). This suggests that the magnitude of exhumation there was not sufficient to expose rocks which have cooled through the AFT and AHe temperature sensitivity ranges (~60-120 °C and ~30-80 °C, respectively). By contrast, Miocene ages from southern Ethiopia clearly record the onset of denudational cooling beginning at ~20-18 Ma in the Chew Bahir Basin (Pik et al., 2008), followed by more widespread rapid cooling beginning at ~14-8 Ma in the Beto Basin and the Amaro Horst (Balestrieri et al., 2016; Philippon et al., 2014). Rapid cooling in central Ethiopia appears to have initiated slightly later at ~7 Ma (Abebe, Balestrieri, & Bigazzi, 2010).

2 Samples and Methods

Ten samples were collected to constrain the low-temperature thermal history of the Lapur Range in northern Turkana (Figures 3 and 4a). Six are from Neoproterozoic-early Paleozoic gneisses and quartzites of the Mozambique Belt, collected at the base of the exposed footwall, ca. ~25-1000m below the Lapur Sandstone nonconformity. An additional four samples were collected from the Upper Cretaceous-Paleogene conglomerates and arkosic sandstones of the Lapur Sandstone; three of these are from an ~E-W striking dry river canyon, the Lokitaung Gorge, forming a footwall transect near-perpendicular to the fault strike to sample progressively shallower-crustal rocks. Sample details, including rock types, coordinates, and elevations are listed in Table 2.

AFT thermochronology is based on the formation of radiation damage trails in apatite, known as fission tracks, that form as a result of spontaneous fission of ^{238}U (e.g. Fleischer et al., 1975; Wagner and Van den Haute, 1992). Fission tracks are sensitive to temperature, remaining relatively stable in apatite below ~60 °C but annealing nearly instantaneously above ~110-120 °C (A. J. W. Gleadow & Duddy, 1981). Between these temperatures, in what is called the partial annealing zone (PAZ), apatite fission tracks anneal (shorten) progressively as a function of time and temperature (Laslett, Green, Duddy, & Gleadow, 1987). The annealing behaviour of fission tracks in apatite is compositionally controlled, with chlorine-rich apatites being more resistant to annealing than their fluorine-rich counterparts (Barbarand, Carter, Wood, & Hurford, 2003; Donelick, O'Sullivan, & Ketcham, 2005). By

combining age and fission track length information, the thermal history of a sample within the PAZ can be reconstructed (Kerry Gallagher, 1995; Ketcham, 2005).

AHe and ZHe thermochronology is based on the production of ^{4}He during the radioactive decay of ^{238}U, ^{235}U and ^{232}Th. ^{4}He is also produced from the radioactive decay of ^{147}Sm, however this generally constitutes <1% of the total ^{4}He, compared to typical He age precisions of a few percent (Kenneth A Farley & Stockli, 2002). When analysing U and Th-rich minerals, such as zircon, the ^{4}He contribution from ^{147}Sm is considered statistically insignificant. However, in some U and Th poor phosphate minerals (e.g. apatite), the consideration of the ^{147}Sm α-source is required. ^{4}He diffusivity is a function of time, temperature, crystal size and accumulated radiation damage (K A Farley, 2000; Reiners & Farley, 2001; Shuster, Flowers, & Farley, 2006). In apatite, ^{4}He diffusion accelerates significantly above ~40 °C and nearly instantaneously above ~80 °C, between which ^{4}He is partially retained (Wolf, Farley, & Kass, 1998). This temperature range is referred to as the apatite partial retention zone (AHe PRZ). The ZHe system is sensitive to higher temperatures, with the zircon partial retention zone (ZHe PRZ) ranging between ~130-200° C (Reiners et al,. 2002; Stockli 2005; Biswas et al. 2007, Wolfe & Stockli 2010).

Multiple studies have shown that He diffusion in both apatite and zircon is dependent on a range of crystallographic and compositional characteristics, sometimes causing He age dispersion. These include U-Th rich inclusions (Danišik et al., 2017; Lippolt, Leitz, Wernicke, & Hagedorn, 1994), which are excluded during the crystal selection procedure, He implantation from external sources for very low U-Th (< 3 ppm) grains (Spiegel, Kohn, Belton, Berner, & Gleadow, 2009), U and Th zonation (Ault & Flowers, 2012; Danišik et al., 2017; Orme, Reiners, Hourigan, & Carrapa, 2015; Tagami, Farley, & Stockli, 2003; Tripathy-Lang, Fox, & Shuster, 2015), and Cl content in apatite (Gautheron, Tassan-Got, Barbarand, & Pagel, 2009). The destructive nature of the AHe and ZHe analytical procedures employed in this study prevent the quantification of the effects of the latter two variables. Three additional variables that may produce intra sample He age variation, i.e. grain size (K A Farley, 2000), accumulated radiation damage (Danišik et al., 2017; Flowers, Ketcham, Shuster, & Farley, 2009; Gautheron et al., 2009; Guenthner, Reiners, Ketcham, Nasdala, & Giester, 2013; Guenthner, Reiners, & Tian, 2014; Nasdala et al., 2004; Shuster & Farley, 2009; Shuster et al., 2006), and crystal breakage (Brown et al., 2013), have been more comprehensively investigated, each of which can lead to over 50% intra-sample age dispersion. Here, we consider grain size, morphology and radiation damage in our thermal history modelling and data interpretation. We use the effective uranium concentration (eU; U + 0.235 x Th), which considers the decay rate and abundance of radiogenic parent elements, as a proxy for α-radiation damage.

A comprehensive review of the AFT, ZHe and AHe methodologies and technical procedures used in this study is given by Gleadow et al. (2015). Apatites and zircons were separated using the standard heavy mineral separation techniques. A synopsis of the AFT, ZHe and AHe analytical protocols are given in the footnotes of Tables 1, 2, and 3, respectively

3 Data

ZHe, AFT and AHe analytical data are listed in Tables 1-3, respectively. A simplified geological map and a cross-section of the Lapur Range, showing sample locations, ages and mean track lengths (MTL) data are presented in Figures 3 and 4a, respectively. Pooled and central AFT ages are indistinguishable within analytical uncertainties and all age values displayed in figures and discussed below are central ages. MTL measurements discussed in the text are reported as un-projected mean 3D lengths, although lengths were *c*-axis projected using the approach of Ketcham et al. (2007b) for thermal history modelling (Section 3.5). All samples yielded sufficient grains for experimentation except for sample 63, where no appropriate apatite or zircon geometries were found for He analyses. None of the AHe or ZHe ages exhibit correlations with either grain size or morphology. All ages are reported to one decimal place in the tables but rounded to whole numbers in the text when 1σ errors are > 5 Ma.

3.1 Zircon (U-Th)/He (ZHe) results

Samples 56, 58 and 61, sampled from within ca. 1000m below the basement nonconformity, yield reproducible ZHe single grain ages within a range of 76 ± 6 Ma to 123 ± 10 Ma. The corresponding weighted mean ZHe ages (4 aliquots each sample) fall within 2σ error, ranging from 93 ± 8 Ma to 104 ± 9 Ma. eU contents of single grain aliquots from these samples are relatively low (90.6-244.3 ppm, Figure 5). Samples 62 and 64, collected ~500 and 25 m below the nonconformity and about ~1.5 km and ~8 km south along-strike of the fault, yield older ZHe weighted mean ages of 223 ± 33 Ma (10 aliquots) and 150 ± 24 Ma (4 aliquots), respectively. Sample 62 yielded nine reproducible single grain ZHe ages (206 ± 17 to 295 ± 24 Ma) with moderate eU concentrations (285.2-592.9 ppm). A tenth single grain analysis from sample 62 yields a much younger single grain age (54 ± 5 Ma) with very high eU (1763.7 ppm; Figure 5), suggesting that the high accumulated radiation damage of this grain has led to decreased He retentivity and a younger ZHe age. By contrast, sample 64 exhibits much greater age dispersion in single grain ZHe ages (92 ± 8 to 211 ± 18 Ma), with younger ages corresponding to higher eU concentrations (ranging between 1069.2 and 550.5 ppm; Figure 5).

Zircon He analyses of Lapur Sandstone samples 65, 66 and 70 yielded concordant weighted mean ages between 404 ± 10 Ma to 436 ± 23 Ma (4 aliquots each; Table 1). Sample 69, collected ~600 m stratigraphically above the basement nonconformity (Figure 4a), yielded a younger Triassic ZHe weighted mean age of 206 ± 31 Ma (3 aliquots). Single grain aliquots of this sample show a marked variation in ZHe ages (164 ± 13 to 271 ± 22 Ma) that are also inversely proportional to eU concentrations (Figure 5; 447.2 to 162.5 ppm).

3.2 Apatite fission track (AFT) results

AFT analyses from Lapur Range basement samples record middle-late Miocene ages (Table 2), showing a trend of apparently older ages closer to the basement nonconformity (14.4 ± 2.6 Ma) and younger ages (9.2 ± 0.5 Ma) further north, at greater crustal depths. MTL are moderate to relatively long and range from 11.9 to 13.2 μm, with moderate standard deviations (Table 2 & Figure 4; 1.93 to 2.69 μm). An exception to this range is sample 63,

which yielded a shorter MTL (11.2 μm) and higher standard deviation (3.4 μm). However, this sample yielded about half the number of confined track measurements (n=55) obtained for other samples (> 100), making its MTL statistically less robust. Chlorine concentrations are consistently low, ranging from 0.01 to 0.20 wt%.

Similar to samples from the underlying basement, AFT ages from the Lapur Sandstone range from 9.0 ± 0.6 to 12.5 ± 2.6 Ma, with MTL of 10.7-12.9 μm and standard deviations of 2.59-3.09 μm (Table 2). Lapur sandstone apatites have low average chlorine compositions, ranging from 0.11 to 0.14 wt%.

3.3 Apatite (U-Th-Sm)/He (ZHe) results

Single grain AHe analyses from Lapur basement samples (56, 58, 61 and 62) yield ages of 3.4 ± 0.3 to 18.2 ± 1.4 Ma, with samples from shallower crustal levels yielding older AHe ages than those from structurally deeper levels (Figures 4a and 6). eU concentrations are relatively low (3.4-28.9 ppm; Table 3) and show no correlation to AHe age.

Lapur sandstone samples yielded similar AHe ages ranging from 3.1 ± 0.3 Ma to 13.4 ± 1.0 Ma, which exhibit a slight negative correlation with eU concentrations (3.9-78.6 ppm).

3.4 Summary of Results

New ZHe, AFT and AHe data from the Lapur Range in the northern Turkana Depression reveal multiple periods of cooling. ZHe results yield a wide range of dispersed ages that, upon further review, exhibit lithological controls, depth dependency and a correlation to accumulated radiation damage. Lapur basement samples collected from the deepest level below the top basement nonconformity (56, 58 and 61) record Cretaceous cooling (~125-75 Ma) through the ZHe PRZ. In contrast, shallower basement samples (62 and 64) yield a wide range of dispersed ages that negatively correlate to eU content (Figure 5). These consist of 4 younger early Late Jurassic-early Paleogene aliquots (54-161 Ma, 1763.7-621.8 ppm) that are in general agreement with ZHe results from deeper basement samples and 10 older Triassic ages (206-295 Ma, 592.9-285.2 ppm). Many authors have noted negative age-eU correlations in previous ZHe studies (e.g. Nasdala et al., 2004; Reiners, 2005; Ketcham et al., 2013), however the exact nature of this relationship remains poorly understood. Guenthner et al. (2013) suggested that the correlation is a product of intra-grain differences in accumulated radiation damage in zircons. In certain cases, such variations result in varying He diffusion rates (or He retentivity) between aliquots, effectively lowering the temperature range of the PRZ for grains with significant radiation damage (e.g. Johnson et al., 2017; Mackintosh et al., 2017). The age-eU relationship observed in shallower Lapur basement samples is interpreted as indicating age dispersion as the product of variations in He diffusivity related to different amounts of α-radiation damage accumulation. In this case, younger aliquots record fully rejuvenated ages despite cooling from the same temperatures as their intra-sample counterparts, as their ZHe PRZ has been effectively lowered by the effects of radiation damage. By contrast, older aliquots record partial overprinting during cooling from temperatures within their ZHe PRZ during a later cooling

phase, such as Cretaceous cooling recorded by deeper basement samples that postdate their Triassic ages.

Lapur Sandstone ZHe ages fall into two populations: twelve zircon ages from samples 65, 66 and 70 yielding late Cambrian to Devonian ages (eU: 61.3-205.7 ppm)and three younger aliquots from sample 69 (eU: 162.5-447.2 ppm), yielding two Jurassic ages and a Permian age. All ZHe ages predate Late Cretaceous-Eocene Lapur Sandstone sedimentation and, thus, record thermal histories inherited from their respective source provenance(s). The low eU concentrations of aliquots from the former group suggest their late Cambrian to Devonian ages may record cooling of the source rocks through the ZHe PRZ during this time. The younger aliquots from sample 69 may record separate periods of cooling through the ZHe PRZ at times corresponding to their respective ZHe ages. Alternatively, their younger ages may be a result radiation damage-related He diffusion that postdates late Cambrian to Devonian cooling recorded by other Lapur Sandstone zircons.

AFT results are summarized in a boomerang plot (Figure 4b), which are often used to illustrate the relationship between fission track age and track length distribution for a set of samples that have experienced a multi-phase thermal history (e.g. Gallagher and Brown, 1997). Samples that record the earlier rapid cooling event yield older AFT ages and long MTL. Whereas, samples that record the subsequent rapid cooling event yield younger AFT ages and long MTL. By contrast, samples which record both thermal events yield intermediate, mixed AFT ages and shortened MTL resulting from partial annealing during the later rapid cooling phase, thus forming a boomerang shape. AFT analyses from this study are interpreted to represent the ascending left-hand portion of a boomerang plot, with basement and Lapur Sandstone samples recording moderate to relatively long MTL (10.7-13.2 μm) and relatively young middle Miocene (9-14 Ma) ages. This suggests that the earlier thermal history of the Lapur Range recorded by ZHe analyses was substantially overprinted by a later cooling phase that, at least partially, postdates the central AFT ages (i.e. < 9 Ma). This is in agreement with their middle Miocene-Pliocene AHe ages (Table 3). Thus, the low-temperature thermochronology data from the Lapur Range indicate that it underwent two episodes of cooling: Cretaceous cooling prior to Lapur Sandstone deposition and a middle Miocene-Pliocene phase.

3.5 Thermal History Reconstructions

In order to quantify time-temperature histories for Lapur Range samples, ZHe, AFT and AHe data were inversely modelled (Figure 6) using *QTQt* (Kerry Gallagher, 2012), with the fission track annealing model of Ketcham et al. (2007a) on the basis of *c*-axis projected track lengths (Ketcham et al., 2007b). Zero termination AHe grains (see Table 3) were omitted during modelling, as the current version of QTQt does not accept this morphology. Radiation damage models were employed for modelling of AHe data (Flowers et al., 2009) and ZHe data (Guenthner et al., 2013) to account for radiation-enhanced annealing as recorded by age-eU relationships. Two time-temperature constraints were applied to the models. The first constraint spans 100-35 Ma, which represents deposition of the Late Cretaceous to middle Paleogene Lapur Sandstone, at which time samples are expected to

have resided at near-surface temperatures (10-30 °C). The second requires the samples to be at surface temperatures (20 ± 10 °C) in the present day.

Samples were grouped by lithology (Lapur basement and Lapur Sandstone) during thermal history modelling. Stratigraphic contacts and bedding relationships (Figure 4a) suggest that the current tilted fault block geometry of the Lapur Range and Turkana Basin is the result of Neogene extension. Therefore, Lapur basement samples were modelled together as a pseudo-vertical profile based on the approximate pre-EARS (i.e. tilt-corrected) position of samples relative to the Cretaceous erosional nonconformity (Figure 4a). Lapur Sandstone samples were also modelled collectively in a similar fashion as basement samples were, whilst allowing for independent pre-depositional t-T paths. This assumes that for any individual sandstone sample, all its respective detrital aliquots experienced a similar pre-depositional thermal history. In the case of samples 65, 66 and 70, the very low inter-aliquot ZHe age dispersion suggests this assumption is valid. This assumption, however, is perhaps invalid for sample 69, whose zircons may record multiple, distinct pre-depositional thermal evolutions (Section 3.4).

Preliminary thermal history modelling of Lapur Sandstone samples suggested a post-depositional thermal history consisting of Late Cretaceous-Paleogene reheating followed by Neogene-Recent cooling to surface temperatures (see below; Section 3.5.1.3 and 3.5.1.4). While the preliminary results were consistent with those of independently modelled basement samples in both character and timing, the maximum paleo-temperatures predicted for the former exceeded those of the basement, which is inconsistent with stratigraphic relationships. Hence, Lapur Sandstone samples were then remodelled with an additional t-T constraint (30-10 Ma, 90-120 °C).

3.5.1 Time-temperature histories

In general, time-temperature reconstructions match the observed data very well. The exception being ZHe data from basement samples 62, 64 and 69 (Figure 6). Sample 64 exhibits a very large spread in aliquot ages that are likely related to radiation damage as discussed above. While the zircon radiation damage accumulation annealing model (ZRDAAM) model of Guenthner et al. (2013) was employed to account for radiation damage during modelling, the model predicts only a moderate amount of inter-grain age variation (~50 Ma), much smaller than observed variations (~120 Ma). Despite these differences, the 1-1 correlation in the predicted vs observed age plot does pass through the spread of aliquots. The ZRDAAM model did a similarly poor job of predicting the oldest ZHe age from sample 69. The largest incongruence however was found between predicted and observed single grain ages for aliquots of sample 62, suggesting that perhaps the ZRDAAM model is unable to fully account for wide ranges of accumulated radiation damage when predicting ZHe ages. Alternatively, the observed dispersion may be the result of intragrain zonation in U and Th. Similar inconsistencies have been reported by Guenthner et al. (2014), where the ZRDAAM model was unable to account completely for intra-sample ZHe age variation.

3.5.1.1 Pre-Cretaceous Thermal History

Thermal history modelling results suggest that the Lapur basement may have undergone a period of gradual heating beginning in the Precambrian, with all but the shallowest sample (64) reaching temperatures > 200 °C by the Early Cretaceous. However, given the total thermal resetting of samples 56, 58 and 61 and almost complete thermal overprinting of samples 62 and 64, the pre-Cretaceous thermal history is not constrained by the data. Eight of the predicted single grain ZHe values for sample 62 are significantly lower than the observed ages (Figure 6), indicating that sample 62 also resided at temperatures within the ZHe PRZ prior to the middle Cretaceous, as opposed to residing at temperatures above the PRZ, as suggested by the thermal history model.

Thermal history reconstructions for the Lapur Sandstone samples consist of an array of best fit t-T paths that seem to suggest monotonic gradual cooling from paleotemperatures ranging between ~20-170 °C in the early Paleozoic and reaching near-surface temperatures by the Upper Cretaceous when detrital zircon grains were redeposited as the Lapur Sandstone (Figure 6).

3.5.1.2 Early-Late Cretaceous Cooling

Between ~120 and 110 Ma, Lapur basement thermal history models record a period of relatively rapid monotonic cooling (~15 °C/Myr), represented by t-T paths for deeper basement samples (56, 58 and 61) which pass through the ZHe PRZ at this time. This thermal history predicts totally reset middle Cretaceous ZHe ages, in agreement with observed data. During this time, shallower samples (62 and 64) cooled from temperatures near or within the upper end of the ZHe PRZ (between ~180-200 °C) to near-surface temperatures. Best-fit t-T paths then transition to a period of very gradual cooling (~0.25 °C/Myr) or thermal stability into the early Late Cretaceous (~90-70 Ma). By the Turonian-early Campanian (~93-75 Ma), the shallowest basement samples were near surface, coinciding with deposition of the overlying Lapur Sandstone.

3.5.1.3 Late Cretaceous-earliest Neogene Reheating

Between ~80 and 60 Ma, all Lapur Range basement and sandstone samples transitioned to a period of moderately rapid reheating (~1.7 °C/km). Thermal history models predict that by the early Miocene (between ~20-14 Ma), samples reached temperatures between 100 and 170°C depending on their relative burial depth. Although time-temperature models appear to suggest that this episode of Paleogene reheating was monotonic and linear, this portion of the Lapur thermal history is not well constrained due to substantial rejuvenation of AFT data prior to Miocene times. Thus, a more complex Paleogene thermal history is possible.

3.5.1.4 Middle Miocene-Pliocene Cooling

Between ~20 to 14 Ma, thermal history models indicate a transition to rapid cooling (6-10 °C/Myr) that is well constrained by the data. Basement samples had passed through the AFT PAZ and AHe PRZ by the end of the Pliocene (between 5-2 Ma) and attained near-

surface temperatures (~20°C) by the present-day. Close inspection reveals that Lapur basement thermal history models appear to suggest that the onset of rapid cooling may have occurred as early as ~20 Ma, although this portion of the thermal history model is below the upper-temperature portion of the PAZ (~100-120°C) and thus not constrained by the basement data. By comparison, thermal history models from the Lapur Sandstone suggest that Neogene cooling likely commenced between ~15 and 14 Ma. This is consistent with observed MTL for these samples, which are of intermediate length (11.8-13.2 μm for samples with a statistically significant number of measurements; Table 2), suggesting that the Lapur Sandstone has not been fully reset and thus records the entire Neogene cooling history from maximum paleotemperatures (< ~120 °C).

3.5.2 Paleogeothermal gradients in Turkana

When interpreting low-temperature (up to ~200°C) thermal history reconstructions to constrain geological processes in the upper crust, temperature is generally used as a proxy for depth (Kohn et al., 2005). Therefore, when making geological inferences from t-T models, accurate assumptions must be made regarding paleo-heat flow to robustly distinguish between tectonic processes, such as long-term denudation and burial rates, and changes in the upper crustal thermal regime (K. Gallagher & Brown, 1999; A. J. W. Gleadow & Brown, 2000).

Heat flow measurements in the Loperot-1 well, ~110 km south of the Lapur Range, indicate that the present day geothermal gradient in Turkana is very high (42 ± 5 °C /km) (Morley, Stone, et al., 1999). This is attributed to a combination of factors including local volcanic activity, very thin crust (~20 km) and, as a consequence, the shallowness of the brittle-ductile transition (Morley, Stone, et al., 1999). The presence of the African Superplume, an elongate mantle thermal anomaly beneath East Africa, may also be a contributing factor to the observed high geothermal gradient (e.g. Hansen et al., 2012). Although it is uncertain when this elevated thermal regime was first initiated, some first-order temporal constraints can nevertheless be made from indirect evidence. Hendrie et al. (1994) showed that the ~35-40 km of extension that occurred since the late Eocene-Oligocene can account for the degree of crustal thinning observed in Turkana (Hendrie et al., 1994). The presence of latest Eocene-Oligocene volcanism in Turkana (Hendrie et al., 1994; Morley et al., 1992; Wescott et al., 1999) and a proposed Oligocene-early Miocene timing for development of the Ethiopian and East African Domes in response to thermal uplift (Pik et al., 2008; Smith & Mosley, 1993; Wichura, Bousquet, Oberhänsli, Strecker, & Trauth, 2010) suggest a late Paleogene arrival of the African Superplume beneath Turkana.

Thus, when interpreting thermal history models in this study and estimating amounts of denudation, a Mesozoic-early Paleogene geothermal gradient of 25-35 ºC/km is used, consistent with the average geothermal gradients for Archean-Proterozoic shields and mobile belts of East Africa (Nyblade, 1990). For late Paleogene-Recent times, a broader geotherm range of 25-45 ºC/km is used to allow for the development of the elevated present-day heat flow and spatial and temporal variation within Turkana.

4 Discussion

The Lapur Range is one of the best-exposed basement blocks in the Turkana Depression, making it an important area to address the question of how this long-lived portion of the EARS has been affected by its superposition with the late Mesozoic-early Cenozoic Anza-South Sudan Rift Systems. Thermochronological data and time-temperature history modelling reveal a complex cooling history spanning Early Cretaceous to Recent time. We suggest that these phases of cooling and reheating are associated with specific periods of regional and local tectonic activity.

4.1 Rapid Early Cretaceous cooling of the Lapur basement

ZHe ages (samples 56, 58 and 61 and high-eU aliquots from samples 62 and 64) and thermal history modelling suggest that the basement rocks of the Lapur Range experienced pronounced and rapid cooling during the Early Cretaceous, beginning sometime between ~120 and 100 Ma. The presence of a top basement erosional unconformity at the contact with the Lapur Sandstone and minor degree of volcanism associated with Anza Rift extension (Morley et al., 1999a) suggest that this cooling was largely a result of denudation.

Wells in the Chalbi Desert (Figure 2) encountered substantial thicknesses of Neocomian-Barremian (up to 695 m) and Aptian (up to 1100 m) sediment (Morley, Bosworth, et al., 1999). The Aptian-Albian was also an important period of source rock deposition in the Muglad Basin of South Sudan (up to 3,353 m thick; Figure 1) (Schull, 1988). Thus, while the Lapur area, according to low-temperature thermochronology data presented here, was experiencing Early Cretaceous exhumation, the Anza and South Sudan Rifts were subsiding. This suggests that the northern Turkana area may have acted as a basement high between the Anza and South Sudan Rifts, as well as an axial sediment source for those grabens. However, the scale of exhumation is substantial. Assuming that erosion was the main cooling mechanism at play, then the ~170-180 ºC of Early Cretaceous cooling recorded by thermal history models would suggest between ~5 and 7 km of denudation (based on a reasonable geothermal gradient of 25-35 ºC/km as discussed earlier). This Early Cretaceous denudation estimate would be significantly reduced if the paleogeothermal gradient in Turkana was higher due to factors such as thermal blanketing effects since removed (e.g. Łuszczak et al., 2017), low thermal conductivity overburden (e.g. Braun et al., 2016) or elevated crustal heat flow that are not taken into consideration.

4.2 Late Cretaceous-earliest Neogene subsidence: Deposition of the Lapur Sandstone and emplacement of the Turkana Volcanics

Lapur basement subsidence began in the early Campanian (ca. 80 Ma), as recorded by thermal history models, with deposition of the Lapur Sandstone (Tiercelin et al., 2012). Continued burial beneath latest Eocene-Oligocene basalt flows and early Miocene rhyolites of the Turkana Volcanics reheated the Lapur basement rocks and overlying Lapur Sandstone, substantially rejuvenating their AFT ages and totally resetting their AHe ages. Thermal history reconstructions indicate that Late Cretaceous-Paleogene reheating was substantial, equivalent to burial beneath ~2-4 km of overburden assuming a geothermal gradient of 25-45

ºC /km. However, only ~500 m of this can be attributed to the Late Cretaceous-early Paleogene Lapur Sandstone in the Lokitaung Gorge area and as little as 100-120 m in the northern Lapur Range (Tiercelin et al., 2012). The remaining overburden likely consisted of latest Eocene-early Miocene Turkana Volcanics, whose lateral equivalents attains thicknesses of up to 3,500 m in the neighboring Lotikipi and Gatome Basins to the west (Wescott et al., 1999).

As the Lapur Range underwent reheating associated with subsidence and burial during the Late Cretaceous to early Paleogene, basement rocks from other parts of Kenya, southern Ethiopia and northern Tanzania appear to have experienced further cooling related to exhumation of the Anza Rift shoulders (Foster and Gleadow, 1992, 1993, 1996; Noble et al., 1997; Spiegel et al., 2007; Philippon et al., 2014; Torres Acosta et al., 2015; Balestrieri et al., 2016). It is still unclear as to how the accommodation space was created in the Lapur area during the Late Cretaceous-early Paleogene. The Lapur Sandstone shows no evidence for rift-related faulting in outcrop, instead having been initially interpreted to represent fluvial deposits that fed laterally into the Anza Rift to the east (Morley et al., 1992). However, a more recent sedimentologic study (Tiercelin et al., 2012) showed the Lapur Sandstone paleodrainage to be far more complex, beginning in a south-southwest direction and later rotating to west-northwest to northeast for much of its history, before returning to south-southwest in the uppermost part of the type-section. Alternating paleoflow directions suggest a poorly understood paleotopographic environment in flux throughout Late Cretaceous-early Paleogene times.

Considering that the South Sudanese and Anza Rifts are thought to potentially link in the Turkana region (e.g. Fairhead, 1988; Bosworth, 1992; Hendrie et al., 1994), our data indicates a surprisingly small degree of Late Cretaceous-early Paleogene subsidence in the Lapur area. This is particularly apparent when considering that total crustal extension across the Anza Rift is estimated to be 60-65 km, equating to a Beta factor (β) of ~2 (Reeves et al., 1987) compared to the relatively minor degree across the Kenyan Rift (β = ~1.15) (Latin, Norry, & Tarzey, 1993). An erosional unconformity in the Lapur Sandstone type-section ~150 m above the basement nonconformity, however, may represent a period of significant erosion and removal of an unknown thickness of sediment (Abdelfettah et al., 2016), perhaps allowing for greater Upper Cretaceous sedimentation undetected by low-temperature thermochronology due to later rejuvenation of the system. The identification of thick piles of sediment in the subsurface of the northern Turkana, Gatome, and Lotikipi Basins (up to 300, 800, and 3,000 m, respectively) thought to possibly correspond to the Lapur Sandstone (Tiercelin et al., 2012; Wescott et al., 1999) suggests that Late Cretaceous-early Paleogene sedimentation may have been far more laterally extensive (~100 km E-W) than outcrop observations would suggest. Tiercelin et al. (2012) proposed a series of en echelon north-dipping normal faults in the Gatome Basin subsurface of suggested mid-Cretaceous age from a reinterpreted seismic line, possibly indicating that active rifting continued elsewhere in northern Turkana during the Cretaceous.

Despite significant effort, the inferred Turkana connection between the Anza and South Sudan Rifts remains speculative and enigmatic. Even if some degree of Cretaceous extension occurred in Turkana, the amount of subsidence indicated by the low-temperature thermal evolution of the Lapur Range in this work is not consistent with a through-going

NW-SE Cretaceous-early Paleogene rift of constant width and geometry. Such an initial setup was employed in the numerical and analog modelling study of Brune et al. (2017), designed to test the hypothesis that the anomalous tectonic and geomorphological evolution of the Turkana Depression resulted from the superposition of Anza-South Sudan and EARS rifting. In that study, Neogene-Recent EARS ~E-W extension was superimposed onto a geometrically homogenous NW-SE trending domain of thinned crust (30 km) extending from the Anza Graben to South Sudan. While their models reproduced some present-day morphological characteristics, such as the development of large escarpments on the NE and SW Turkana Depression margins, and depicted an eastward propagation of rifting in southern Ethiopia consistent with current thinking (e.g. Ebinger et al., 2000; Balestrieri et al. 2016). However, their model also predicted an east-to-west propagation of extension in Turkana that is opposite to that observed (e.g. Morley et al., 1992; Morley, Stone et al., 1999; Wescott et al., 1999).

Instead, our findings suggest that later Paleogene tectonics may have played a more pivotal role in modifying the Turkana crustal architecture than perhaps thought. As pointed out by Tiercelin et al. (2012), the abrupt termination of Lapur Sandstone sedimentation coincided with the first eruptions between 45-35 Ma of plume-generated volcanics in southern Ethiopia (Ebinger & Sleep, 1998; Ebinger et al., 1993; R. M. George & Rogers, 2002), reaching northern Turkana by 37-35 Ma (Ebinger et al., 1993; R. George, Rogers, & Kelley, 1998; McDougall & Brown, 2009; Pik et al., 2008). The simultaneous arrival of a shallow plume beneath the Turkana Depression and an end to Lapur Sandstone deposition perhaps suggests that dynamic topography was responsible for ending early Paleogene subsidence in the Lapur Range. Thermal uplift has also been suggested to have caused inversion in the Muruanachok Basin (Morley, Stone, et al., 1999), whose eroded basin infill remnants consist of Cretaceous?-Paleogene sandstone (Figure 2) (Morley et al., 1992; Tiercelin et al., 2012).

During the late Paleogene, widespread extension is thought to have continued in the Turkana Depression resulting in a series of basins running from the Sudanese-Ethiopian border, through Turkana and reactivated portions of the eastern Anza Rift (Figure 1) (Bosworth, 1992; Hendrie et al., 1994). Locally, late Paleogene extension was expressed by the development of the Lotikipi, Gatome, North Lokichar and Lokichar Basins (Morley, Stone, et al., 1999; Wescott et al., 1999), marking a period of significant crustal thinning in Turkana (Hendrie et al., 1994).

4.3 Middle Miocene initiation of extension in the northern Turkana Basin

Beginning in the middle Miocene (~14 Ma), the Lapur basement and overlying Lapur Sandstone underwent a period of rapid cooling. The observed paleo-depth - AFT data relationship, whereby rocks at greater stratigraphic or structural depths yield younger AFT ages, longer MTL and lower standard deviations (Figure 4a), is indicative of denudation-related cooling. Thus, we interpret the observed mid-Miocene cooling of the Lapur Range to reflect flexural isostatic uplift of the MRL footwall in response to normal displacement of the hanging wall rocks. Since the MRL master fault accommodated the vast majority of Neogene extension across the basin (Abdelfettah et al., 2016), the onset of MRL isostatic footwall

uplift at ~14 Ma likely indicates a middle Miocene initiation of extension across the entire northern Turkana Basin. This is supported by the presence of a pile of westward thickening sedimentary rocks overlying the Turkana Volcanics within the northern Turkana Basin hanging wall, thought to be of upper Miocene-Pliocene age (Morley, Stone, et al., 1999; Wescott et al., 1999). Our interpretation is therefore in strong agreement with the rift propagation model of Morley et al. (1999b), whereby the mid-Miocene, extension had migrated from western Turkana to the basins underlying Lake Turkana. A middle Miocene phase of extension has also been suggested for numerous other EARS basins elsewhere in the eastern Turkana Depression and the flanks of the Kenyan and Ethiopian Domes (Figure 2). This suggests a simultaneous migration of EARS rifting both north- and southward into the thicker crustal domains of southern Ethiopia and central Kenya at this time (Bonini et al., 2005).

Low-temperature thermochronology data indicate that basement samples from the deepest pre-EARS crustal levels (samples 56, 58 and 61) cooled from ~110-120 °C to surface temperatures by the Pleistocene-Holocene. Depending on spatial and temporal variations in Turkana geothermal gradients during the last ~14 Ma, this degree of cooling is consistent with ~2-4 km of footwall uplift in the Lapur Range. By comparison, previous AFT studies in the Kenya Rift have reported maximum middle Miocene-Recent denudational cooling associated with EARS-related extension of between 40-60 °C (Foster & Gleadow, 1996; Torres Acosta et al., 2015).

4.4 Lapur AFT data in a regional context: How has rift superposition affected the Turkana lithosphere's response to EARS extension?

AFT analyses from the Lapur Range yield the first Neogene apparent ages that record cooling directly related to the morphotectonic evolution of the EARS in Kenya (Figure 7). This finding is surprising considering the northern Turkana Basin exhibits a similar duration of EARS extension (mid Miocene-Recent), amount of extension (≤ 10 km) and similar style of faulting to many other basins in the Kenyan Rift (Ebinger et al., 2000; Morley, Ngenoh, et al., 1999; Morley, Stone, et al., 1999). The previous lack of Neogene AFT ages suggests that exhumation rates in the Kenyan Rift, south of Turkana, have been insufficient to exhume deep-seated basement rocks that record EARS-related cooling through the PAZ. The greater degree of Neogene cooling recorded in the Lapur Range is therefore attributed to either increased footwall uplift due to a difference in lithospheric response during rifting, or a relatively higher geothermal gradient in Turkana, resulting in greater cooling for an equivalent amount of denudation, or a combination of the two. A third possibility, whereby crustal heat-flow in the Turkana region decreased since the mid-Miocene could also result in a greater-degree of observed cooling. However, continued volcanic activity into late Pleistocene time (Morley, Stone, et al., 1999) and further Neogene-Pliocene extension throughout much of Turkana, resulting in further crustal thinning, makes this explanation highly unlikely.

Egan (1992) proposed that the amplitude of isostatic footwall uplift is dependent on the flexural rigidity of the lithosphere undergoing extension (Figure 8). The inherited thin crust and resulting high heat flow of the Turkana Depression, both in part products of its

earlier Cretaceous-Paleogene rifting history, would have amplified its lithospheric response to EARS-related crustal extension, as predicted by thin plate flexure theory (Walcott, 1970). Hendrie et al. (1994), using the flexural cantilever model of continental extension (e.g. Kusznir and Ziegler, 1992), calculated an effective elastic thickness (T_e) estimate of just 3.5 km for the Turkana region, compared to ~25 km estimated for the central Kenyan Rift (Bechtel, Forsyth, & Swain, 1987; Ebinger, Deino, Drake, & Tesha, 1989). Such a large difference in T_e would allow the Turkana lithosphere to undergo approximately twice the amount of footwall uplift than the more rigid central Kenyan lithosphere, assuming a similar amount of basin extension (~10 km; Figure 8).

While elevated crustal heat flow in Turkana is evidenced by a geothermal gradient of 4.2 °C/100 m from the Loperot-1 well (Morley, Stone, et al., 1999), similarly high geothermal gradients have been observed in multiple drill holes and wells from the central Kenya Rift (~3-6 °C/100 m) (Wheildon, Morgan, Williamson, Evans, & Swanberg, 1994), suggesting that a difference in heat flow alone cannot account for the greater degree of cooling observed in the Lapur Range. Thus, we believe that the larger amount of Miocene cooling in the Lapur Range is largely the result of increased isostatic uplift in the MRL footwall due to the low effective elastic thickness in the Turkana Depression.

5 Conclusions

ZHe, AFT and AHe analyses have been applied to 10 samples from the Lapur Range, an uplifted basement block in the footwall of the basin-bounding MRL Fault of the northern Turkana Basin. These data combined with inverse thermal history modelling reveal the following:

1. Basement rocks of the Lapur Range show a pronounced phase of Early Cretaceous (between 100-120 Ma) cooling consistent with ~5-7 km of denudation. Coeval subsidence in the adjacent Anza and South Sudan Rifts suggests that the northern Turkana region may have acted as a basement high separating these rift systems and provided a local source for axially fed sediment.
2. The Lapur region transitioned to a period of reheating in the Late Cretaceous, between ca. 80 Ma and 20 Ma, coinciding with the deposition of ~500m of Upper Cretaceous-Eocene Lapur Sandstone and emplacement of up to 3.5 km of late Eocene-early Miocene Turkana Volcanics.
3. EARS-related faulting commenced in the Lapur area in the mid-Miocene at ~ 14 Ma, with the formation of the northern Turkana Basin bounding MRL Fault, coeval with rift initiation in other parts of eastern Turkana and southern Ethiopia.
4. Cooling rates associated with EARS-related flexural isostatic footwall uplift are significantly higher in the Turkana region compared to the Kenyan Rift, further south. This is best explained by the comparatively thin crust and high heat flow of the Turkana Depression, lowering the effective elastic thickness of its lithosphere. These crustal features are inherited from the Cretaceous-Paleogene rifting history of this region and amplified isostatic footwall uplift in response to extension.

Acknowledgements

We note that there are no data sharing issues since all numerical information is provided in the tables. Funding for this research was provided through Australian Research Council grant DP130101610. SCB received additional support from the MIFRS and MIRS scholarships and the Baragwanath Geology Research Scholarship awarded by the University of Melbourne. The University of Melbourne Thermochronology Lab receives infrastructure support under the AuScope program of NCRIS. This work was carried out with permission of the Kenyan National Commission for Science, Technology and Innovation under the terms of Research Permits NCSTI/P/13/4850/25 and NACOSTI/P/16/4850/13111. We would like to thank Dr Christopher Nyamai and Dr Daniel Ichang'i at the Department of Geology, University of Nairobi for their assistance in facilitating this project. The cooperation and hospitality of Richard and Meave Leakey, Francis Ekai, Moses Loparakuo Lenina and other Turkana Basin Institute staff were critical in carrying out fieldwork for this project. Technical assistance by Abaz Alimanovic for (U-Th)/He and Graham Hutchinson for electron microprobe analyses are greatly appreciated. We thank Chris Morley for his valuable suggestions and insight into East African geology, as well as Ulrich A Glasmacher and Editor Nathan Niemi for their constructive and helpful reviews.

Figure Captions

Figure 1. Regional map of East Africa showing the location of the Turkana Depression in relation to the distribution of Cretaceous, Paleogene and Neogene-Recent rift basins. The broad, uplifted Ethiopian and East African Domes are outlined in light blue. The Kenyan Dome, a subsidiary of the East African Dome, is outlined in dark blue. (after Hendrie et al., 1994)

Figure 2. Simplified geological map of the Turkana Depression showing the distribution of latest Cretaceous?-Paleogene to Recent extensional basins (adapted from Kazmin, 1972; GMRD-Sudan, 1981; BEICIP, 1987; Lehto et al., 2014; Philippon et al., 2014; Balestrieri et al., 2016) . Chronograms at the top and right sides of the geological map depict the spatial-temporal relationship of Cenozoic extension (after Torres Acosta et al., 2015). Solid blue bars show documented periods of extension from previous sedimentary and structural geology studies, while possible periods of extension that are poorly constrained by data are shown as hashed blue bars. Periods of rift-related rapid cooling from low-temperature thermochronology studies are shown with red stars with black outlines. A red star with a grey outline marks cooling observed in this study. Information was compiled from the following sources: (1) this study, (2) Torres Acosta et al. (2015), (3) Morley et al. (1999b), (4) Foster and Gleadow (1996), (5) Spiegel et al. (2007), (6) Wescott et al. (1999), (7) Ebinger et al. (1993), (8) Pik et al. (2008), (9) Philippon et al. (2014), (10) Woldegabriel et al. (1990), (11) Ebinger et al. (2000), (12) Zanettin et al. (1983), (13) Mugisha et al. (1997), (14) Morley et

al. (1999c), (15) Lippard (1972), (16) Hautot et al. (2000), (17) Balestrieri et al. (2016) and (18) Bonini et al. (2005).

Figure 3. Simplified geological map of the Lapur Range with sample localities (blue dots) and low-temperature thermochronology results of this study. Refer to Figure 2 for geographic location. ZHe (blue), AFT and mean track length (MTL; see Section 2) (black), and AHe data (red) for each sample are presented in white boxes. The approximate location of the MRL normal fault is illustrated with a black hashed line. The location of seismic line TVK-10 (Figure 4a) is illustrated in black (Wescott et al., 1999). Adapted from Walsh and Dodson (1969); Abdelfettah et al. (2016).

Figure 4. a) Sample locations (blue dots) projected on a geological cross-section of the Lapur Range and northern Turkana Basin adapted from Wescott et al. (1999). ZHe, AFT, AHe and confined fission track length distributions are shown for each sample. n = number of confined track length measurements included in the histogram and MTL result for that sample. Dashed lines in upper cross-section represent inferred unit boundaries from seismic interpretation of Wescott et al. (1999). Grey hashed lines on lower cross-section represent the relative stratigraphic depth of samples in relation to the basement-Lapur Sandstone nonconformity, prior to Miocene faulting and block rotation. Note that the dips of the MRL Fault and unit boundaries appear steeper due to the slight vertical exaggeration applied (true dips are ~65° E for the MRL Fault and ~15° W for the unit boundaries). Geological units and sample data follow the key in Figure 3. **b)** Lapur AFT data (blue circles) plotted as AFT age versus MTL, forming the ascending portion a boomerang plot (see Section 3.4). Red circles represent AHe ages.

Figure 5. Plot of single grain ZHe ages versus effective uranium (eU) content of Lapur Range samples, with the approximate duration of relevant major regional tectonothermal events recorded in East Africa shown in grey. Basement samples 56, 58 and 61, which, prior to the mid-Miocene extension and block tilting were at structurally deepest in the basement levels, record Cretaceous single grain ZHe ages that are likely related to coeval Cretaceous-Paleogene Anza-South Sudanese rifting. The remaining samples display a range of Cambrian to Paleogene single grain ZHe ages. Some samples show a negative correlation between single grain ages and the eU content (red line), which suggests that the intermediate Permian-Triassic ZHe ages of samples 62, 64 and 69 are products of increased He diffusivity due to radiation damage effects and, thus, do not record distinct tectonothermal event(s) at those times.

Figure 6. ZHe and AHe data and inverse thermal history models of Lapur basement samples (left side and bottom model) and Lapur Sandstone samples (right side and top model). Single sample ZHe and AHe data are arranged by relative stratigraphic depth relative to the top basement nonconformity prior to mid-Miocene tilting of fault blocks, with deepest samples at the bottom. Ternary plots for ZHe (left column) and AHe (right column) data, generated with *HelioPlot* (Vermeesch 2010), display the relationship between ages and U, Th and He concentrations for individual aliquots. The colour of single grain AHe ages shifts towards

green with increasing Sm content. Corresponding central He ages (± 1σ) are listed above the ternary diagrams. The approximate temperature sensitivity range for each thermochronometer is highlighted in the thermal models. Applied time-temperature constraints are marked by black boxes (see Section 3.5). The best-fit t-T path for each individual sample is shown in a color corresponding to that of the line displayed above its He data. In each vertical profile the envelope of acceptable t-T paths for the uppermost (blue path) and lowermost (red path) sample shown by light blue and purple envelopes, respectively. A plot of values predicted by thermal models versus observed values are shown for each model. ZHe data = inverted triangles, AHe data = upright triangles and AFT data = circles.

Figure 7. Image showing Lapur Range apatite fission track (AFT) ages within a regional context. **a)** Interpolation of Kenyan AFT data from previous studies (Gleadow, 1980; Foster and Gleadow, 1992, 1996; Wagner et al., 1992b; Spiegel et al., 2007; Majer-Kielbaska, 2015; Torres Acosta et al., 2015) and data presented in this paper superimposed on a DEM image. Samples from the Tanzanian Craton exhibit AFT ages >250 Ma, while most of Kenya records Late Cretaceous-early Paleogene AFT ages related to uplift and denudation of the Cretaceous-Paleogene Anza Rift margin. All samples from the Lapur Range of the Turkana Depression (this study; red circles) exhibit young Miocene AFT ages. The small orange area in the Kenyan Rift, just north of the Tanzanian Craton, corresponds to samples that yield Eocene-Oligocene AFT ages, interpreted to represent cooling from the lower PAZ during Neogene EARS-related extension (Torres Acosta et al., 2015). Sample localities are represented by green dots. **b)** Boomerang plot of AFT ages versus MTL from all Kenyan (see references for Figure 7a), Ethiopian (Abebe et al., 2010; Balestrieri et al., 2016; Philippon et al., 2014), and Tanzania (Noble, 1997; Noble et al., 1997; van der Beek et al., 1998). AFT studies. See Section 3.4 for a description of a Boomerang Plot.

Figure 8. Plot of isostatic footwall uplift (km) versus effective elastic thickness (T_e) for 10 km of extension, illustrating how the flexural isostatic response to extension depends on lithospheric rigidity (adapted from Egan, 1992). Effective elastic thickness estimates for Turkana (Hendrie et al., 1994) and the Kenyan Rift (Ebinger et al., 1989) are plotted, illustrating that after 10 km of extension, the relatively low T_e of the Turkana lithosphere allows for twice the amount of isostatic footwall uplift than the thicker, cooler central Kenyan lithosphere.

References

Abdelfettah, Y., Tiercelin, J., Tarits, P., Hautot, S., Maia, M., & Thuo, P. (2016). Subsurface structure and stratigraphy of the northwest end of the Turkana Basin, Northern Kenya Rift, as revealed by magnetotellurics and gravity joint inversion. *Journal of African Earth Sciences*, *119*, 120–138. https://doi.org/10.1016/j.jafrearsci.2016.03.008

Abebe, T., Balestrieri, M. L., & Bigazzi, G. (2010). The Central Main Ethiopian Rift is younger than 8 Ma: confirmation through apatite fission-track thermochronology. *Terra Nova*, *22*(6), 470–476. https://doi.org/10.1111/j.1365-3121.2010.00968.x

Arambourg, C., & Wolff, R. G. (1969). Nouvelles données paléontologique sur l'âge des "Gres du Lubur" (Turkana Grits) al'ouest du lac Rodolphe. *Comptes Rendus Société Géologique de France*, *9*, 190–202.

Ault, A. K., & Flowers, R. M. (2012). Is apatite U-Th zonation information necessary for accurate interpretation of apatite (U-Th)/He thermochronometry data? *Geochimica et Cosmochimica Acta*, *79*, 60–78. https://doi.org/10.1016/j.gca.2011.11.037

Baker, B. H., & Wohlenberg, J. (1971). Structure and Evolution of the Kenya Rift Valley. *Nature*, *229*, 538–542.

Balestrieri, M. L., Bonini, M., Corti, G., Sani, F., & Philippon, M. (2016). A refinement of the chronology of rift-related faulting in the Broadly Rifted Zone, southern Ethiopia, through apatite fission-track analysis. *Tectonophysics*, *671*, 42–55. https://doi.org/10.1016/j.tecto.2016.01.012

Barbarand, J., Carter, A., Wood, I., & Hurford, T. (2003). Compositional and structural control of fission-track annealing in apatite. *Chemical Geology*, *198*(1–2), 107–137. https://doi.org/10.1016/S0009-2541(02)00424-2

Bauer, F. U., Glasmacher, U. A., Ring, U., Karl, M., Schumann, A., & Nagudi, B. (2013). Tracing the exhumation history of the Rwenzori Mountains, Albertine Rift, Uganda, using low-temperature thermochronology. *Tectonophysics*, *599*, 8–28. https://doi.org/10.1016/j.tecto.2013.03.032

Bauer, F. U., Karl, M., Glasmacher, U. A., Nagudi, B., Schumann, A., & Mroszewski, L. (2012). Journal of African Earth Sciences The Rwenzori Mountains of western Uganda – Aspects on the evolution of their remarkable morphology within the Albertine Rift. *Journal of African Earth Sciences*, *73–74*, 44–56. https://doi.org/10.1016/j.jafrearsci.2012.07.001

Bechtel, T. D., Forsyth, D. W., & Swain, C. J. (1987). Mechanisms of isostatic compensation in the vicinity of the East African Rift, Kenya. *Geophysical Journal of the Royal Astronomical Society*, *90*, 445–465. https://doi.org/10.1111/j.1365-246X.1987.tb00734.x

Begg, G. C., Griffin, W. L., Natapov, L. M., O'Reilly, S. Y., Grand, S. P., O'Neill, C. J., … Bowden, P. (2009). The lithospheric architecture of Africa: Seismic tomography, mantle petrology, and tectonic evolution. *Geosphere*, *5*(1), 23–50. https://doi.org/10.1130/GES00179.1

BEICIP. (1987). Geological Map of Kenya. Nairobi: Ministry of Energy and Regional Development.

Bellieni, G., Justin Visentin, E., Zanettin, B., Piccirillo, E. M., Radicati di Brozolo, F., & Rita, F. (1981). Oligocene transitional tholeiitic magmatism in Northern turkana

(Kenya): Comparison with the Coeval Ethiopian volcanism. *Bulletin Volcanologique*, *44*(3), 411–427. https://doi.org/10.1007/BF02600573

Benoit, M. H., Nyblade, A. A., & Pasyanos, M. E. (2006). Crustal thinning between the Ethiopian and East African plateaus from modeling Rayleigh wave dispersion. *Geophysical Research Letters*, *33*(13). https://doi.org/10.1029/2006GL025687

Biswas, S., Coutand, I., Grujic, D., Hager, C., Stockli, D., & Grasemann, B. (2007). Exhumation and uplift of the Shillong plateau and its influence on the eastern Himalayas: New constraints from apatite and zircon (U-Th-[Sm])/He and apatite fission track analyses. *Tectonics*, *26*. https://doi.org/10.1029/2007TC002125

Bonini, M., Corti, G., Innocenti, F., Manetti, P., Mazzarini, F., Abebe, T., & Pecskay, Z. (2005). Evolution of the Main Ethiopian Rift in the frame of Afar and Kenya rifts propagation. *Tectonics*, *24*(1), n/a-n/a. https://doi.org/10.1029/2004TC001680

Boone, S. C., Seiler, C., Reid, A. J., Kohn, B., & Gleadow, A. (2016). An Upper Cretaceous paleo-aquifer system in the Eromanga Basin of the central Gawler Craton, South Australia: evidence from apatite fission track thermochronology. *Australian Journal of Earth Sciences*, *63*(3), 315–331. https://doi.org/10.1080/08120099.2016.1199050

Bosworth, W. (1992). Mesozoic and early Tertiary rift tectonics in East Africa. *Tectonophysics*, *209*(1–4), 115–137. https://doi.org/10.1016/0040-1951(92)90014-W

Bosworth, W., & Morley, C. K. (1994). Structural and stratigraphic evolution of the Anza rift, Kenya. *Tectonophysics*, *236*(1–4), 93–115. https://doi.org/10.1016/0040-1951(94)90171-6

Braun, J., Stippich, C., & Glasmacher, U. A. (2016). The effect of variability in rock thermal conductivity on exhumation rate estimates from thermochronological data. *Tectonophysics*, *690*, 288–297. https://doi.org/10.1016/j.tecto.2016.09.027

Brown, R. W., Beucher, R., Roper, S., Persano, C., Stuart, F., & Fitzgerald, P. (2013). Natural age dispersion arising from the analysis of broken crystals. Part I: Theoretical basis and implications for the apatite (U-Th)/He thermochronometer. *Geochimica et Cosmochimica Acta*, *122*(120), 478–497. https://doi.org/10.1016/j.gca.2013.05.041

Brown, R. W., Rust, D. J., Summerfield, M. A., Gleadow, A. J. W., & De Wit, M. C. J. (1990). An Early Cretaceous Phase of Accelerated Erosion on the South-Western Margin of Africa: Evidence from Apatite Fission Track Analysis and the Offshore Sedimentary Record. *International Journal of Radiation Applications and Instrumentation*, *Part D*, *17*(3), 339–350.

Browne, S. E., & Fairhead, J. D. (1983). Gravity study of the Central African Rift system: A model of continental disruption 1. The Ngaoundere and Abu Gabra Rifts. *Tectonophysics*, *94*(1–4), 187–203. https://doi.org/10.1016/0040-1951(83)90016-1

Brune, S., Corti, G., & Ranalli, G. (2017). Controls of inherited lithospheric heterogeneity on rift linkage: Numerical and analog models of interaction between the Kenyan and Ethiopian rifts across the Turkana depression. *Tectonics*, 1–30. https://doi.org/10.1002/2017tc004739

Chorowicz, J. (2005). The East African rift system. *Journal of African Earth Sciences*, *43*, 379–410. https://doi.org/10.1038/215578a0

Danišik, M., McInnes, B. I. A., Kirkland, C. L., McDonald, B. J., Evans, N. J., & Becker, T.

(2017). Seeing is believing: Visualization of He distribution in zircon and implications for thermal history reconstruction on single crystals. *Science Advances*, *3*, 1–9.

Donelick, R. A., O'Sullivan, P. B., & Ketcham, R. A. (2005). Apatite Fission-Track Analysis. *Reviews in Mineralogy and Geochemistry*, *58*(1), 49–94. https://doi.org/10.2138/rmg.2005.58.3

Dunkelman, T. J., Rosendahl, B. R., & Karson, J. A. (1989). Structure and stratigraphy of the Turkana rift from seismic reflection data. *Journal of African Earth Sciences*, *8*(2–4), 489–510. https://doi.org/10.1016/S0899-5362(89)80041-7

Ebinger, C. J., Deino, A. L., Drake, R. E., & Tesha, A. L. (1989). Chronology of Volcanism and Rift Basin Propagation: Rungwe Volcanic Province, East Africa. *Journal of Geophysical Research*, *94*(B11), 15,785-15,803.

Ebinger, C. J., & Sleep, N. H. (1998). Cenozoic magnatism throughout east Africa resulting from impact of a single plume. *Nature*, *395*, 788–791.

Ebinger, C. J., Yemane, T., Harding, D., Tesfaye, S., Kelley, S., & Rex, D. C. (2000). Rift deflection , migration , and propagation □: Linkage of the Africa. *GSA Bulletin*, *112*(2), 163–176.

Ebinger, C. J., Yemane, T., Woldegabriel, G., Aronson, J. L., & Walter, R. C. (1993). Late Eocene-Recent volcanism and faulting in the southern main Ethiopian rift. *Journal of the Geological Society*, *150*(1), 99–108. https://doi.org/10.1144/gsjgs.150.1.0099

Egan, S. S. (1992). The flexural isostatic response of the lithosphere to extensional tectonics. *Tectonophysics*, *202*(2–4), 291–308. https://doi.org/10.1016/0040-1951(92)90115-M

Fairhead, J. D. (1988). Mesozoic plate tectonic reconstructions of the central South Atlantic Ocean: The role of the West and Central African rift system. *Eisevier Science Publishers B.V.. Amsterdam*, *155*, 181–191. https://doi.org/10.1016/0040-1951(88)90265-X

Farley, K. A. (2000). Helium diffusion from apatite: General behavior as illustrated by Durango fluorapatite. *Journal of Geophysical Research*, *105*(B2), 2903–2914.

Farley, K. A., & Stockli, D. F. (2002). (U-Th)/ He Dating of Phosphates: Apatite, Monazite, and Xenotime. *Reviews in Mineralogy and Geochemistry*, *48*(1), 559–577. https://doi.org/10.2138/rmg.2002.48.15

Farley, K. A., Wolf, R. A., & Silver, L. T. (1996). The effects of long alpha-stopping distances on (U-Th)/He ages. *Geochimica et Cosmochimica Acta*, *60*(21), 4223–4229. https://doi.org/10.1016/S0016-7037(96)00193-7

Feibel, C. S., Brown, F. H., & McDougall, I. (1989). Stratigraphic context of fossil hominids from the Omo group deposits: Northern Turkana Basin, Kenya and Ethiopia. *American Journal of Physical Anthropology*, *78*(4), 595–622. https://doi.org/10.1002/ajpa.1330780412

Feinstein, S., Eyal, M., Kohn, B. P., Steckler, M. S., Ibrahim, K. M., Moh'd, B. K., & Tian, Y. (2013). Uplift and denudation history of the eastern Dead Sea rift fl ank , SW Jordan *Tectonics*, *32*, 1513– Evidence from apatite fi ssion tra 1528. https://doi.org/10.1002/tect.20082

Fleischer, R., Price, P., & Walker, R. (1975). *Nuclear Tracks in Solids: principles and applications*. Berkeley: University of California Press.

Flowers, R. M., Ketcham, R. A., Shuster, D. L., & Farley, K. A. (2009). Apatite (U-Th)/He

thermochronometry using a radiation damage accumulation and annealing model. *Geochimica et Cosmochimica Acta*, *73*(8), 2347–2365. https://doi.org/10.1016/j.gca.2009.01.015

Foster, D. A., & Gleadow, A. J. W. (1992). The morphotectonic evolution of rift-margin mountains in central Kenya: Constraints from apatite fission-track thermochronology. *Earth and Planetary Science Letters*, *113*(1–2), 157–171. https://doi.org/10.1016/0012-821X(92)90217-J

Foster, D. A., & Gleadow, A. J. W. (1993). Episodic Denudation in East Africa: A Legacy of Intracontinental Tectonism. *Geophysical Research Letters*, *20*(21), 2395–2398.

Foster, D. A., & Gleadow, J. W. (1996). Structural framework and denudation history of the flanks of the Kenya and Anza Rifts , East Africa. *Tectonics*, *15*(2), 258–271. https://doi.org/10.1029/95TC02744

Galbraith, R. F. (2005). *Statistics for fission track analysis*. CRC Press.

Gallagher, K. (1995). Evolving temperature histories from apatite fission-track data. *Earth and Planetary Science Letters*, *136*(3–4), 421–435.

Gallagher, K. (2012). Transdimensional inverse thermal history modeling for quantitative thermochronology. *Journal of Geophysical Research: Solid Earth*, *117*. https://doi.org/10.1029/2011JB008825

Gallagher, K., & Brown, R. (1997). The onshore record of passive margin evolution. *Journal of the Geological Society, London*, *154*, 451–457. https://doi.org/10.1144/gsjgs.154.3.0451

Gallagher, K., & Brown, R. (1999). Denudation and uplift at passive margins: the record on the Atlantic Margin of southern Africa. *Philosophical Transactions of the Royal Society London A: Mathematical, Physical and Engineering Sciences*, *357*, 835–859. https://doi.org/10.1098/rsta.1999.0354

Gautheron, C., Tassan-Got, L., Barbarand, J., & Pagel, M. (2009). Effect of alpha-damage annealing on apatite (U-Th)/He thermochronology. *Chemical Geology*, *266*, 157–170. https://doi.org/10.1016/j.chemgeo.2009.06.001

George, R. M., & Rogers, N. W. (2002). Plume dynamics beneath the African plate inferred from the geochemistry of the Tertiary basalts of southern Ethiopia. *Contribution to Mineralogy and Petrology*, *144*, 286–304. https://doi.org/10.1007/s00410-002-0396-z

George, R., Rogers, N., & Kelley, S. (1998). Earliest magnatism in Ethiopia: Evidence for two mantle plumes in one flood basalt province. *Geology*, *26*(10), 923–926.

Gleadow, A. J. W., Gleadow, S. J., Belton, D. X., Kohn, B. P., Krochmal, M. S., & Brown, R. W. (2009). Coincidence mapping – a key strategy for the automatic counting of fission tracks in natural minerals. *Geological Society of London Special Publications, Thermochronological Methods: From Palaeotemperature Constraints to Landscape Evolution Models.*, *324*, 25–36. https://doi.org/10.1144/SP324.2

Gleadow, A., Harrison, M., Kohn, B., Lugo-zazueta, R., & Phillips, D. (2015). The Fish Canyon Tuff a new look at an old low-temperature thermochronology standard. *Earth and Planetary Science Letters*, *424*, 95–108. https://doi.org/10.1016/j.epsl.2015.05.003

Gleadow, A. J. W. (1980). Fission track age of the KBS Tuff and associated hominid remains in northern Kenya. *Nature*, *284*, 225–230. https://doi.org/10.1038/284225a0

Gleadow, A. J. W., & Brown, R. W. (2000). Fission track thermochronology and the long-term denudational response to tectonics. *Geomorphology and Global Tectonics*, (May), 57–75. Retrieved from y:%5CARCHIV_GEOWATT%5CPaper%5CPaper_archiviert%5CGleadow_1999_Wiley_FissionTrackAnalysis.pdf

Gleadow, A. J. W., & Duddy, I. R. (1981). A Natural Long-Term Track Annealing Experiment for Apatite. *Nuclear Tracks*, *5*(1–2), 169–174.

GMRD-Sudan. (1981). Geological Map of the Sudan. Khartoum: Geological & Mineral Resources Department (G. M. R. D.) Sudan.

Greene, L. C., Richards, D. R., & Johnson, R. A. (1991). Crustal structure and tectonic evolution of the anza rift, northern Kenya. *Tectonophysics*, *197*(2–4), 203–211. https://doi.org/10.1016/0040-1951(91)90041-P

Guenthner, W. R., Reiners, P. W., Ketcham, R. A., Nasdala, L., & Giester, G. (2013). Helium diffusion in natural zircon: radiation damage, anisotropy, and the interpretation of zircon (U-TH)/He thermochronology. *American Journal of Science*, *313*(3), 145–198. https://doi.org/10.2475/03.2013.01

Guenthner, W. R., Reiners, P. W., & Tian, Y. (2014). Interpreting date-eU correlations in zircon (U-Th)/He datasets: A case study from the Longmen Shan, China. *Earth and Planetary Science Letters*, *403*(OCTOBER), 328–339. https://doi.org/10.1016/j.epsl.2014.06.050

Guiraud, R., & Bosworth, W. (1997). Senonian basin inversion and rejuvenation of rifting in Africa and Arabia - synthesis and implications to plate scale tectonics. *Tectonophysics*, *282*, 39–82.

Guiraud, R., & Maurin, J.-C. (1992). Early Cretaceous rifts of Western and Central Africa: an overview. *Tectonophysics*, *213*, 153–168.

Hansen, S. E., Nyblade, A. A., & Benoit, M. H. (2012). Mantle structure beneath Africa and Arabia from adaptively parameterized P-wave tomography: Implications for the origin of Cenozoic Afro-Arabian tectonism. *Earth and Planetary Science Letters*, *319–320*, 23–34. https://doi.org/10.1016/j.epsl.2011.12.023

Hasebe, N., Barbarand, J., Jarvis, K., Carter, A., & Hurford, A. J. (2004). Apatite fission-track chronometry using laser ablation ICP-MS. *Chemical Geology*, *207*(3), 134–145.

Hautot, S., Tarits, P., Whaler, K., Le Gall, B., Tiercelin, J.-J., & Le Turdu, C. (2000). Deep structure of the Baringo Rift Basin (central Kenya) from three-dimensional magnetotelluric imaging: Implications for rift evolution. *Journal of Geophysical Research*, *105*(B10), 23,493-23,518. https://doi.org/10.1029/2000JB900213

Hendrie, D. B., Kusznir, N. J., Morley, C. K., & Ebinger, C. J. (1994). Cenozoic extension in northern Kenya: a quantitative model of rift basin development in the Turkana region. *Tectonophysics*, *236*(1–4), 409–438. https://doi.org/10.1016/0040-1951(94)90187-2

Henry, W. J., Mechie, J., Maguire, P. K. H., Khan, M. A., Prodehl, C., Keller, G. R., & Patel, J. (1990). A Seismic Investigation of the Kenya Rift Valley. *Geophysical Journal International*, *100*(1), 107–130. https://doi.org/10.1111/j.1365-246X.1990.tb04572.x

Hourigan, J. K., Reiners, P. W., & Brandon, M. T. (2005). U-Th zonation-dependent alpha-ejection in (U-Th)/He chronometry. *Geochimica et Cosmochimica Acta*, *69*(13), 3349–3365. https://doi.org/10.1016/j.gca.2005.01.024

Ibrahim, A. E., Ebinger, C. J., & Fairhead, J. D. (1991). Interpretation of the Central African Rift system in Sudan based on new gravity and aeromagnetic data. *EOS*, *462*.

Johnson, J. E., Flowers, R. M., Baird, G. B., & Mahan, K. H. (2017). "Inverted" zircon and apatite (U–Th)/He dates from the Front Range, Colorado: High-damage zircon as a low-temperature (<50 ◦C) thermochronometer. *Earth and Planetary Science Letters*, *466*, 80–90. https://doi.org/10.1016/j.epsl.2017.03.002

Kasanzu, C. H. (2016). Apatite fission track and (U-Th)/He thermochronology from the Archean Tanzania craton: Contributions to cooling histories of Tanzanian basement rocks. *Geoscience Frontiers*, 1–9. https://doi.org/10.1016/j.gsf.2016.09.007

Kasanzu, C. H., Linol, B., de Wit, M. J., Brown, R., Persano, C., & Stuart, F. M. (2016). From source to sink in central Gondwana: Exhumation of the Precambrian basement rocks of Tanzania and sediment accumulation in the adjacent Congo basin. *Tectonics*, *35*(9), 2034–2051. https://doi.org/10.1002/2016TC004147

Kazmin, V. (1972). Geological Map of Ethiopia. Addis Ababa: Geological Survey of Ethiopia, Ministry of Mines.

Ketcham, R. A. (2005). Forward and Inverse Modeling of Low- Temperature Thermochronometry Data. *Reviews in Mineralogy and Geochemistry*, *58*, 275–314. https://doi.org/10.2138/rmg.2005.58.11

Ketcham, R. A., Carter, A., Donelick, R. A., Barbarand, J., & Hurford, A. J. (2007a). Improved measurement of fission-track annealing in apatite using c-axis projection. *American Mineralogist*, *92*(5–6), 789–798. https://doi.org/10.2138/am.2007.2280

Ketcham, R. A., Carter, A., Donelick, R. A., Barbarand, J., & Hurford, A. J. (2007b). Improved modeling of fission-track annealing in apatite. *American Mineralogist*, *92*, 799–810. https://doi.org/10.2138/am.2007.2281

Ketcham, R. A., Guenthner, W. R., & Reiners, P. W. (2013). Geometric analysis of radiation damage connectivity in zircon, and its implications for helium diffusion. *American Mineralogist*, *98*(2–3), 350–360. https://doi.org/10.2138/am.2013.4249

Kohn, B. P., Gleadow, A. J. W., Brown, R. W., Gallagher, K., Lorencak, M., & Noble, W. P. (2005). Visualizing Thermotectonic and Denudational Histories Using Apatite Fission Track Thermochronology. *Reviews in Mineralogy and Geochemistry*, *58*, 527–565. https://doi.org/10.2138/rmg.2005.58.20

Kreuser, T. (1995). Rift to drift evolution in Permian-Jurassic basins of East Africa. *Geological Society, London, Special Publication*, *80*(1), 297–315.

Kröner, a, & Stern, R. J. (2005). Pan-African Orogeny. *Encyclopedia 0f Geology*, *1*(2004), 1–12. https://doi.org/10.1016/S1342-937X(05)70162-3

Kusznir, N. J., & Ziegler, P. A. (1992). The mechanics of continental extension and sedimentary basin formation: A simple-shear flexural cantilever model, *215*, 117–131.

Laslett, G. M., Green, P. F., Duddy, I. R., & Gleadow, A. J. W. (1987). Thermal annealing of fission tracks in apatite 2 . A quantitative analysis. *Chemical Geology (Isotope Geoscience Section)*, *65*, 1–13. https://doi.org/10.1016/0168-9622(87)90057-1

Latin, D., Norry, M. J., & Tarzey, R. J. E. (1993). Magmatism in the gregory rift, East Africa: Evidence for melt generation by a plume. *Journal of Petrology*, *34*(5), 1007–1027. https://doi.org/10.1093/petrology/34.5.1007

Lehto, T., Westerhof, A. B., Lehtonen, M. I., Manninen, T., Mäkitie, H., Virransalo, P., … Elepu, D. (2014). Geological Map of Uganda, Scale 1:1 000 000. Espoo, Finland: Geological Survey of Finland.

Lippard, S. J. (1972). *Stratigraphy and structure of the Elgeyo escarpment southern Kamasia Hills and adjoining regions, Rift Valley Province, Kenya*. Royal Holloway, University of London.

Lippolt, H. J., Leitz, M., Wernicke, R. S., & Hagedorn, B. (1994). (Uranium + thorium)/helium dating of apatite: experience with samples from different geochemical environments. *Chemical Geology*, *112*(1–2), 179–191. https://doi.org/10.1016/0009-2541(94)90113-9

Lisker, F., Brown, R., & Fabel, D. (2003). Denudational and thermal history along a transect across the Lambert Graben , northern Prince Charles Mountains , Antarctica , derived from apatite fission track thermochronology, *22*(5). https://doi.org/10.1029/2002TC001477

Łuszczak, K., Persano, C., Braun, J., & Stuart, F. M. (2017). How local crustal thermal properties influence the amount of denudation derived from low-temperature thermochronometry. *Geology*, *45*(9), 779–782. https://doi.org/10.1130/G39036.1

Mackintosh, V., Kohn, B., Gleadow, A., & Tian, Y. (2017). Phanerozoic Morphotectonic Evolution of the Zimbabwe Craton: Unexpected Outcomes From a Multiple Low-Temperature Thermochronology Study. *Tectonics*, *36*, 1–24. https://doi.org/10.1002/2017TC004703

Maguire, P. K. H., Swain, C. J., Masotti, R., & Khan, M. A. (1994). A crustal and uppermost mantle cross-sectional model of the Kenya Rift derived from seismic and gravity data. *Tectonophysics*, *236*(1–4), 217–249. https://doi.org/10.1016/0040-1951(94)90178-3

Majer-Kielbaska, D. A. (2015). *Low temperature thermochronology of the northernmost Mozambique Belt, Kenya*. University of Melbourne.

Mbede, E., Andriessen, P., Delvaux, D., & van der Beek, P. (1998). Denudation history of the Malawi and Rukwa Rift flanks (East African Rift System) from apatite fission track thermochronology. *Journal of African Earth Sciences*, *26*(3), 363–385.

McDougall, I., & Brown, F. H. (2009). Timing of volcanism and evolution of the northern Kenya Rift. *Geological Magazine*, *146*(1), 34–37. https://doi.org/10.1017/S0016756808005347

McDowell, F. W., McIntosh, W. C., & Farley, K. A. (2005). A precise 40Ar-39Ar reference age for the Durango apatite (U-Th)/He and fission track dating standard. *Chemical Geology*, *214*(3), 249–263.

Mechie, J., Keller, G. R., Prodehl, C., Gaciri, S., Braile, L. W., Mooney, W. D., … Sandmeier, K.-J. (1994). Crustal structure beneath the Kenya Rift from axial profile data. *Tectonophysics*, *236*, 179–200.

Morley, C. K., Bosworth, W., Day, R. A., Lauck, R., Bosher, R., Stone, D. M., … Bassett, N. (1999). Geology and Geophysics of the Anza Graben. In C. K. Morley (Ed.), *Geoscience of Rift Systems-Evolution of East Africa: AAPG Studies in Geology No. 44* (pp. 67–90).

Morley, C. K., Ngenoh, D. K., & Ego, J. K. (1999). Introduction to the East African Rift System. In C. K. Morley (Ed.), *Geoscience of Rift Systems-Evolution of East Africa:*

AAPG Studies in Geology No. 44 (pp. 1–18).
Morley, C. K., Stone, D. M., Harper, R. M., & Wigger, S. T. (1999). Geology and Geophysics of the Western Turkana Basins , Kenya. In C. K. Morley (Ed.), *Geoscience of Rift Systems—Evolution of East Africa: AAPG Studies in Geology No. 44* (pp. 19–54).
Morley, C. K., Wescott, W. a., Stone, D. M., Harper, R. M., Wigger, S. T., & Karanja, F. M. (1992). Tectonic evolution of the northern Kenyan Rift. *Journal of the Geological Society*, *149*(3), 333–348. https://doi.org/10.1144/gsjgs.149.3.0333
Mugisha, F., Ebinger, C. J., Strecker, M., & Pope, D. (1997). Two-stage rifting in the Kenya rift: implications for half-graben models. *Tectonophysics*, *278*, 63–81.
Nasdala, L., Reiners, P. W., Garver, J. I., Kennedy, A. K., Stern, R. A., Balan, E., & Wirth, R. (2004). Incomplete retention of radiation damage in zircon from Sri Lanka. *American Mineralogist*, *89*(1), 219–231. https://doi.org/10.2138/am-2004-0126
Noble, W. P. (1997). *Post Pan African Tectonic Evolution of Eastern Africa: An Apatite Fission Track Study*. La Trobe University.
Noble, W. P., Foster, D. A., & Gleadow, A. J. W. (1997). The post-Pan-African thermal and extensional history of crystalline basement rocks in eastern Tanzania. *Tectonophysics*, *275*(4), 331–350. https://doi.org/10.1016/S0040-1951(97)00026-7
Nyblade, A. A. (1990). Terrestrial heat flow in east and southern Africa. *Journal of Geophysical Research: Solid Earth*, *95*(B11), 17371–17384.
O'Connor, P. M., Sertich, J. J. W., & Manthi, F. K. (2011). A pterodactyloid pterosaur from the Upper Cretaceous Lapurr sandstone, West Turkana, Kenya. *Anais Da Academia Brasileira de Ciencias*, *83*(1), 309–315. https://doi.org/10.1590/S0001-37652011000100019
Orme, D. A., Reiners, P. W., Hourigan, J. K., & Carrapa, B. (2015). Effects of inherited cores and magmatic overgrowths on zircon (U-Th)/He ages and age-eU trends from Greater Himalyan sequence rocks, Mount Everest region, Tibet. *Geochemistry Geophysics Geosystems*, *16*, 2499–2507. https://doi.org/10.1002/2015GC005818
Paton, C., Hellstrom, J., Paul, B., Woodhead, J., & Hergt, J. (2011). Iolite: Freeware for the visualisation and processing of mass spectrometric data. *Journal of Analytical Atomic Spectrometry*, *26*, 2508–2518. https://doi.org/10.1039/c1ja10172b
Philippon, M., Corti, G., Sani, F., Bonini, M., Balestrieri, M., Molin, P., … Cloetingh, S. (2014). Evolution, distribution, and characteristics of rifting in southern Ethiopia. *Tectonics*, *33*, 1–24. https://doi.org/10.1002/2013TC003430
Pik, R., Marty, B., Carignan, J., Yirgu, G., & Ayalew, T. (2008). Timing of East African Rift development in southern Ethiopia Implication fo of topography. *Geology*, *36*(2), 167–170. https://doi.org/10.1130/G24233A.1
Reeves, C. V., Karanja, F. M., & MacLeod, I. N. (1987). Geophysical evidence for a failed Jurassic rift and triple junction in Kenya. *Earth and Planetary Science Letters*, *81*(2–3), 299–311. https://doi.org/10.1016/0012-821X(87)90166-X
Reiners, P. W. (2005). Zircon (U-Th)/He Thermochronometry. *Reviews in Mineralogy and Geochemistry*, *58*, 151–179. https://doi.org/10.2138/rmg.2005.58.6
Reiners, P. W., & Farley, K. A. (2001). Influence of crystal size on apatite (U-Th)/ He thermochronology: an example from the Bighorn Mountains, Wyoming. *Earth and Planetary Science Letters*, *188*, 413–420.

Schull, T. J. (1988). Rift Basins of Interior Sudan: Petroleum Exploration and Discovery, *72*(10), 1128–1142.

Seiler, C., Fletcher, J. M., Kohn, B. P., Gleadow, A. J. W., & Raza, A. (2011). Low - temperature thermochronology of northern Baja California , Mexico : Decoupled sli exhumation gradients and delayed onset of oblique rifting across the Gulf of California. *Tectonics*, *30*(1). https://doi.org/10.1029/2009TC002649

Seiler, C., Kohn, B., & Gleadow, A. (2014). Apatite fission track analysis by LA-ICP-MS: An evaluation of the absolute dating approach. In *International Conference on Thermochronology*.

Shuster, D. L., & Farley, K. A. (2009). The influence of artificial radiation damage and thermal annealing on helium diffusion kinetics in apatite. *Geochimica et Cosmochimica Acta*, *73*(1), 183–196. https://doi.org/10.1016/j.gca.2008.10.013

Shuster, D. L., Flowers, R. M., & Farley, K. A. (2006). The influence of natural radiation damage on helium diffusion kinetics in apatite. *Earth and Planetary Science Letters*, *249*(3–4), 148–161. https://doi.org/10.1016/j.epsl.2006.07.028

Sippel, J., Meeßen, C., Cacace, M., Mechie, J., Fishwick, S., Heine, C., Scheck-Wenderoth, M., & Strecker, M. R. (2017). The Kenya rift revisited: insights into lithospheric strength through data-driven 3-D gravity and thermal modelling. *Solid Earth*, *8*, 45–81. https://doi.org/10.5194/se-8-45-2017

Smith, M., & Mosley, P. (1993). Crustal Heterogeneity and Basement Influence on the Development of the Kenya Rift, East Africa. *Tectonics*, *12*(2), 591–606.

Spiegel, C., Kohn, B., Belton, D., Berner, Z., & Gleadow, A. (2009). Apatite (U-Th-Sm)/He thermochronology of rapidly cooled samples: The effect of He implantation. *Earth and Planetary Science Letters*, *285*(1–2), 105–114. https://doi.org/10.1016/j.epsl.2009.05.045

Spiegel, C., Kohn, B. P., Belton, D. X., & Gleadow, A. J. W. (2007). Morphotectonic evolution of the central Kenya rift flanks: Implications for late Cenozoic environmental change in East Africa. *Geology*, *35*(5), 427–430. https://doi.org/10.1130/G23108A.1

Stockli, D. F. (2005). Application of low-temperature thermochronology to extensional tectonic settings. *Reviews in Mineralogy and Geochemistry*, *58*(1), 411–448.

Sullivan, P. B. O. Y., Mitchell, M. M., Sullivan, A. J. O., Kohn, B. P., & Gleadow, A. J. W. (2000). Thermotectonic history of the Bassian Rise , Australia : implications fo breakup of eastern Gondwana along Australia ' s southeastern margins, *182*, 31–47.

Tagami, T., Farley, K. A., & Stockli, D. F. (2003). (U-Th)/He geochronology of single zircon grains of known Tertiary eruption age. *Earth and Planetary Science Letters*, *207*(1–4), 57–67. https://doi.org/10.1016/S0012-821X(02)01144-5

Tiercelin, J. J., Potdevin, J. L., Thuo, P. K., Abdelfettah, Y., Schuster, M., Bourquin, S., … Ruffet, G. (2012). Stratigraphy, sedimentology and diagenetic evolution of the Lapur Sandstone in northern Kenya: Implications for oil exploration of the Meso-Cenozoic Turkana depression. *Journal of African Earth Sciences*, *71–72*, 43–79. https://doi.org/10.1016/j.jafrearsci.2012.06.007

Torres Acosta, V., Bande, A., Sobel, E. R., Parra, M., Schildgen, T. F., Stuart, F., & Strecker, M. R. (2015). Cenozoic extension in the Kenya Rift from low-temperature

thermochronology: Links to diachronous spatiotemporal evolution of rifting in East Africa. *Tectonics*, *34*(12), 2367–2386. https://doi.org/10.1002/2015TC003949

Tripathy-Lang, A., Fox, M., & Shuster, D. L. (2015). Zircon 4He/3He thermochronometry. *Geochimica et Cosmochimica Acta*, *166*, 1–14. https://doi.org/10.1016/j.gca.2015.05.027

Unrug, R. (1997). Rodinia to Gondwana: The geodynamic map of Gondwana supercontinent assembly. *GSA Today*, *7*(1). https://doi.org/10.2460/javma.242.12.1666

van der Beek, P., Mbede, E., Andriessen, P., & Delvaux, D. (1998). Denudation history of the Malawi and Rukwa Rift flanks (East African Rift system) from apatite fission track thermochronology. *Journal of African Earth Sciences*, *26*(3), 363–385. https://doi.org/10.1016/S0899-5362(98)00021-9

Vermeesch, P. (2009). RadialPlotter: A Java application for fission track, luminescence and other radial plots. *Radiation Measurements*, *44*(4), 409–410.

Vermeesch, P. (2010). HelioPlot, and the treatment of overdispersed (U-Th-Sm)/He data. *Chemical Geology*, *271*(3–4), 108–111. https://doi.org/10.1016/j.chemgeo.2010.01.002

Wagner, G., & Van den Haute, P. (1992). *Fission-Track Dating*. Dordrecht: Kluwer Academic Publishers.

Wagner, M., Altherr, R., & Van Den Haute, P. (1992). Apatite fission-track analysis of Kenyan basement rocks: constraints on the thermotectonic evolution of the Kenya dome. A reconnaissance study. *Tectonophysics*, *204*(1–2), 93–110. https://doi.org/10.1016/0040-1951(92)90272-8

Walcott, R. I. (1970). Flexural Rigidity, Thickness, and Viscosity of the Lithosphere. *Journal of Geophysical Research*, *75*(20), 3941–3954. https://doi.org/10.1029/JB075i020p03941

Walsh, J., & Dodson, R. G. (1969). Geology of Northern Turkana, Degree Sheets 1, 2, 9, and 10. Geological Survey of Kenya.

Wescott, W. A., Wigger, S. T., Stone, D. M., & Morley, C. K. (1999). Geology and Geophysics of the Lotikipi Plain. *Geoscience of Rift Systems-Evolution of East Africa*, (44), 55–66.

Wheildon, J., Morgan, P., Williamson, K. H., Evans, T. R., & Swanberg, C. A. (1994). Heat flow in the Kenya rift zone. *Tectonophysics*, *236*(1–4), 131–149. https://doi.org/10.1016/0040-1951(94)90173-2

Wichura, H., Bousquet, R., Oberhänsli, R., Strecker, M. R., & Trauth, M. H. (2010). Evidence for middle Miocene uplift of the East African Plateau. *Geology*, *38*(6), 543–546. https://doi.org/10.1130/G31022.1

Wolf, R. A., Farley, K. A., & Kass, D. M. (1998). Modeling of the temperature sensitivity of the apatite (U – Th)/He thermochronometer. *Chemical Geology*, *148*, 105–114.

WoldeGabriel, G., Aronson, J. L., & Walter, R. C. (1990). Geochronology and rift basin development in the central sector of the Main Ethiopian Rift. *Geological Society of America Bulletin*, *102*, 439–485. https://doi.org/10.1130/0016-7606(1990)102<0439

Wolfe, M. R., & Stockli, D. F. (2010). Zircon (U-Th)/He thermochronometry in the KTB drill hole, Germany, and its implications for bulk He diffusion kinetics in zircon. *Earth and Planetary Science Letters*, *295*(1–2), 69–82. https://doi.org/10.1016/j.epsl.2010.03.025

Wolfenden, E., Ebinger, C., Yirgu, G., Deino, A., & Ayalew, D. (2004). Evolution of the

northern Main Ethiopian rift: birth of a triple junction. *Earth and Planetary Science Letters*, *224*(1–2), 213–228. https://doi.org/10.1016/j.epsl.2004.04.022

Zanettin, B., Justin Visentin, E., Bellieni, G., Piccirillo, E. M., & Francesca, R. (1983). The volcanism of the North Turkana Basin, Kenya: age, succession and structural evolution. *Bulletin Des Centres de Recherches Exploration-Production Elf-Aquitaine*, *7*, 249–255.

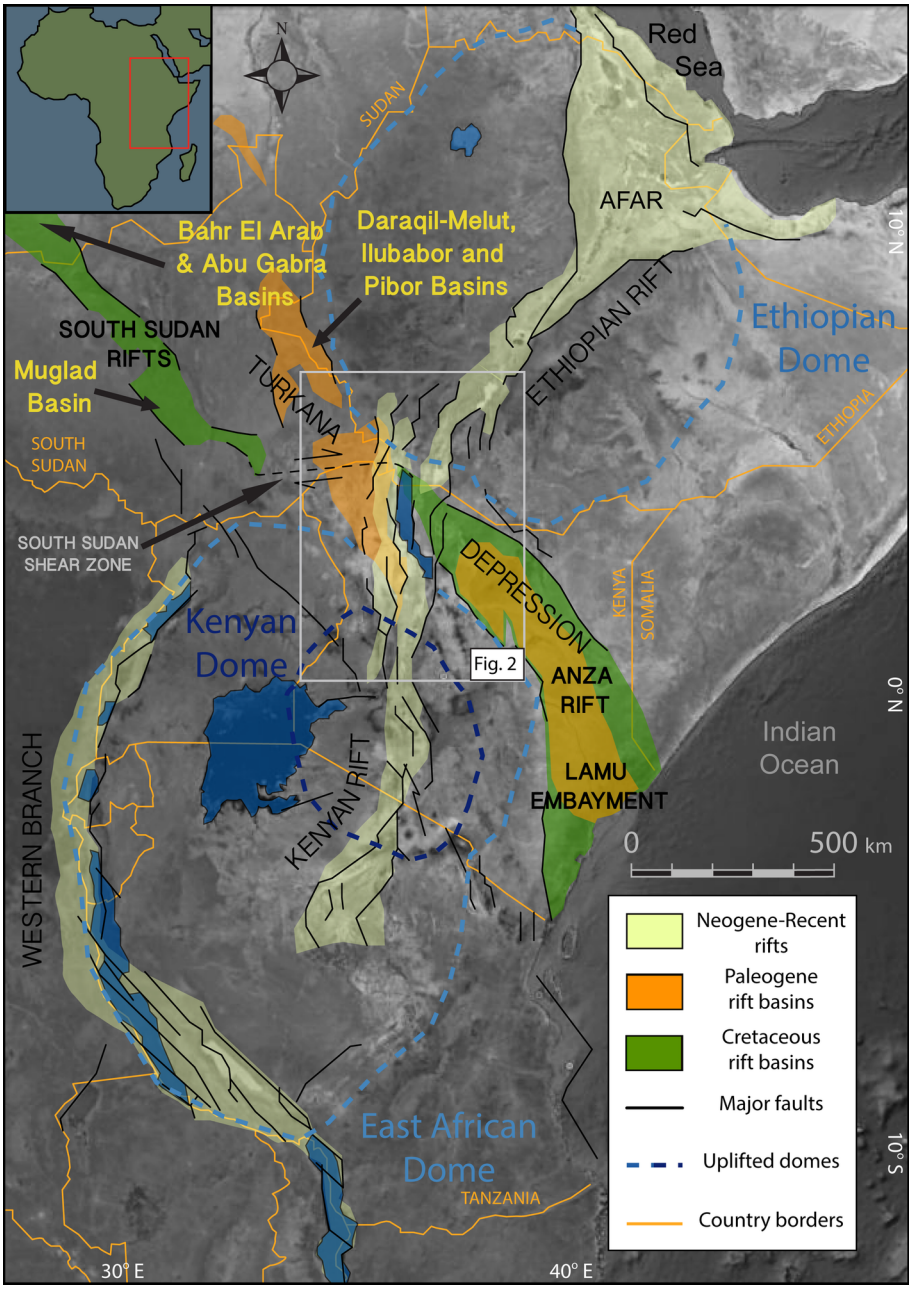

2017TC004575-f01-z-.tif

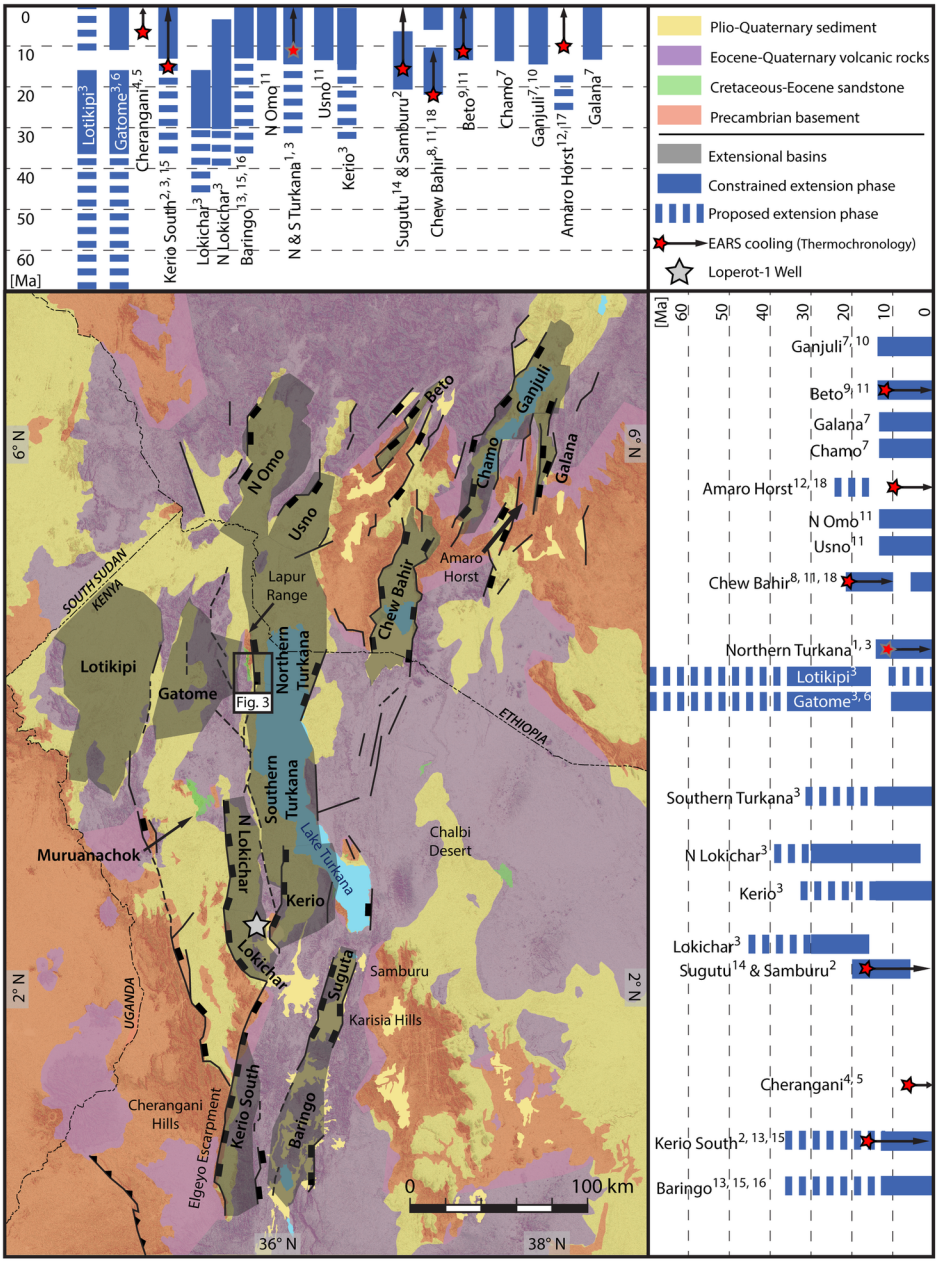

2017TC004575-f02-z-.tif

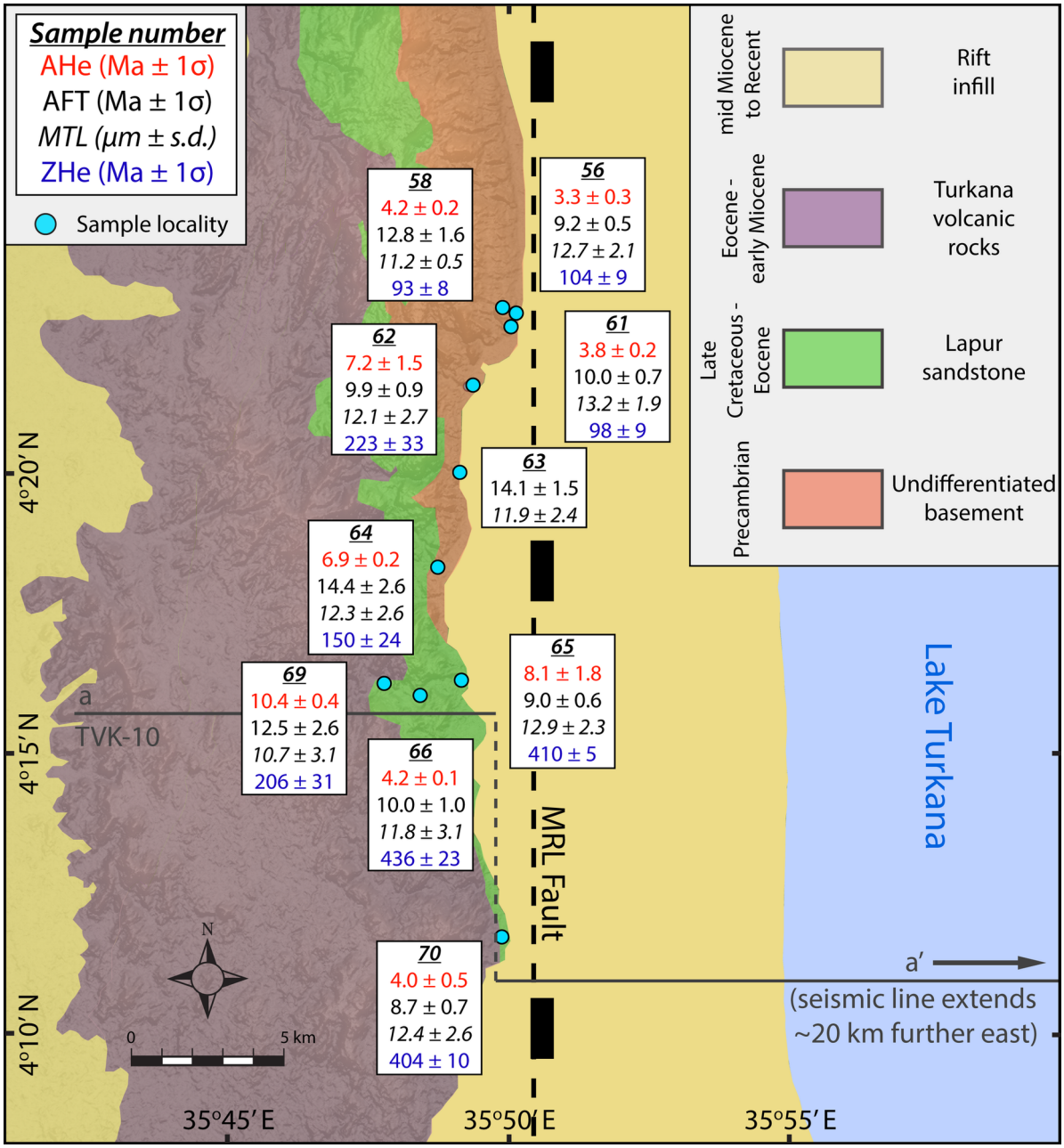

2017TC004575-f03-z-.tif

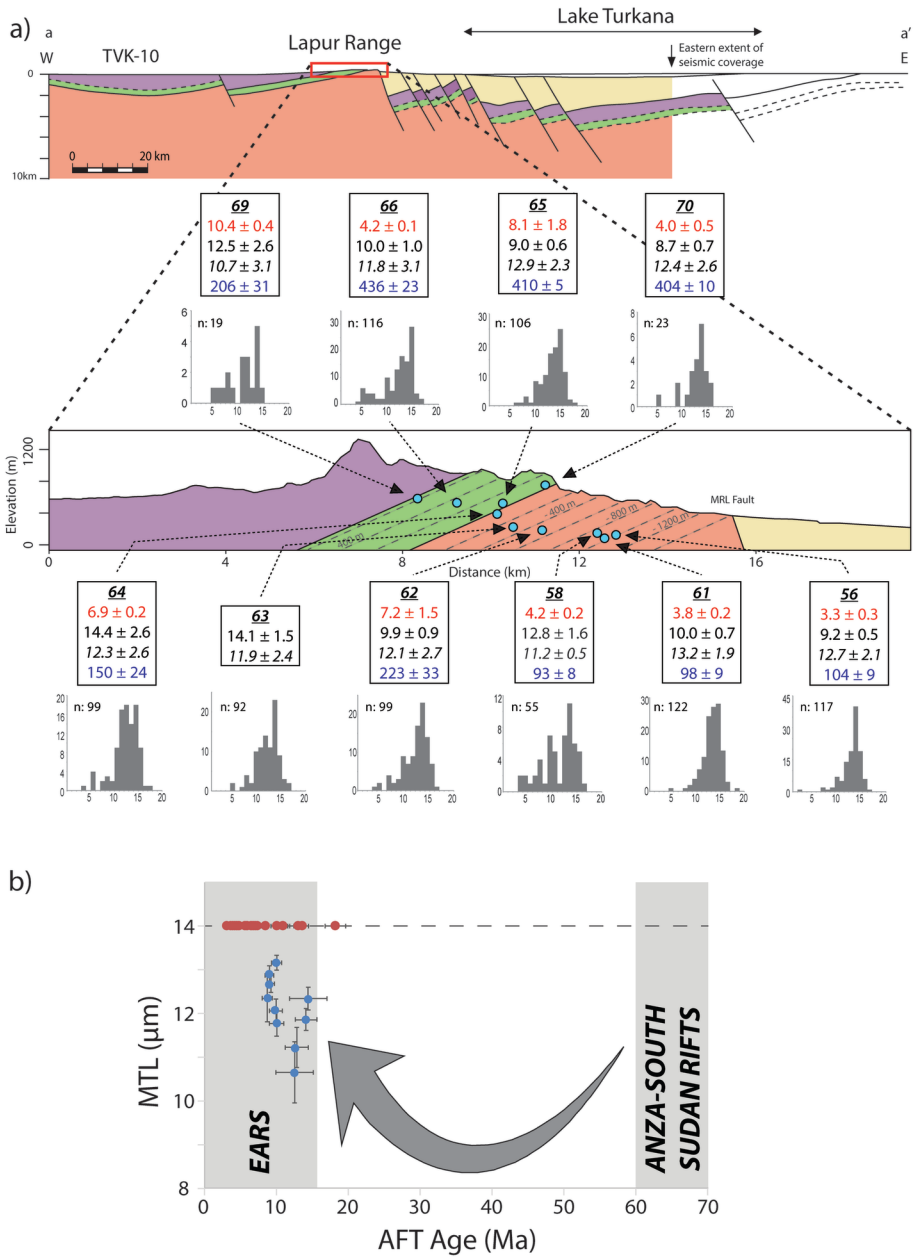

2017TC004575-f04-z-.tif

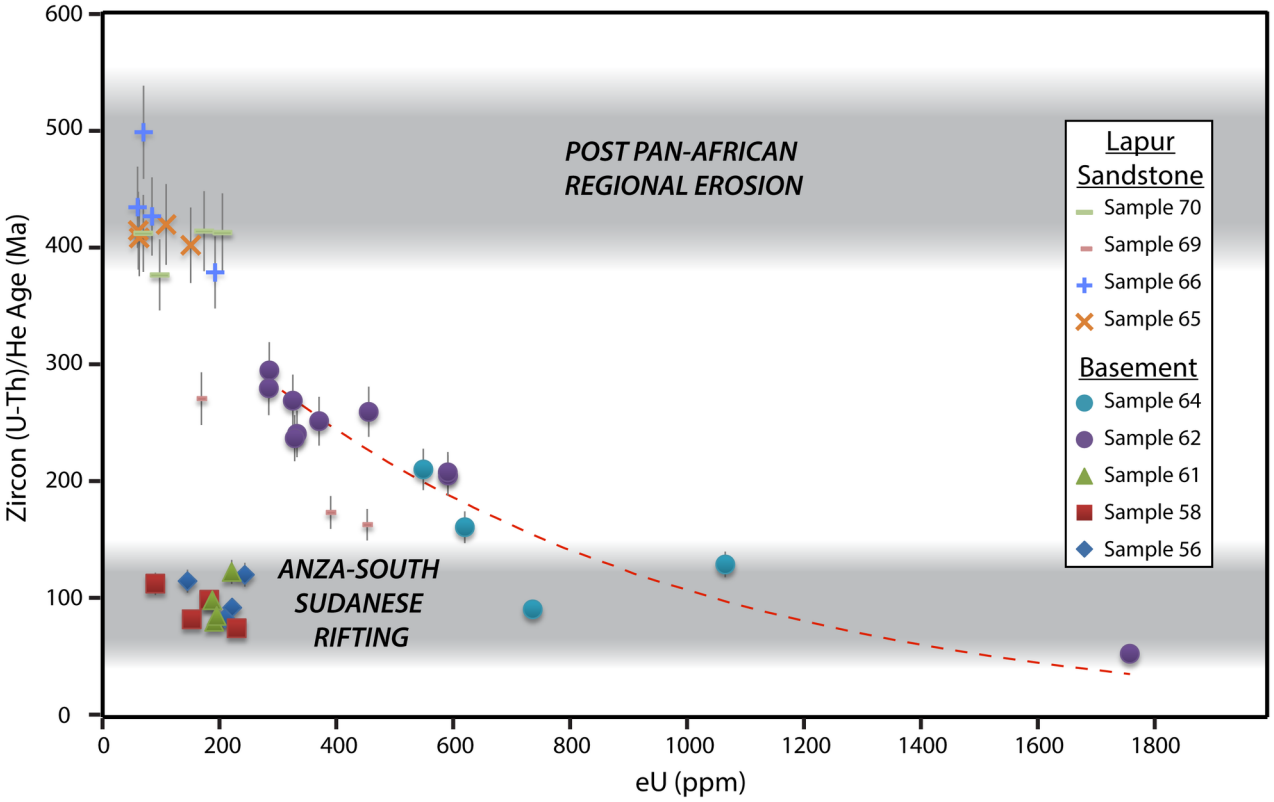

2017TC004575-f05-z-.tif

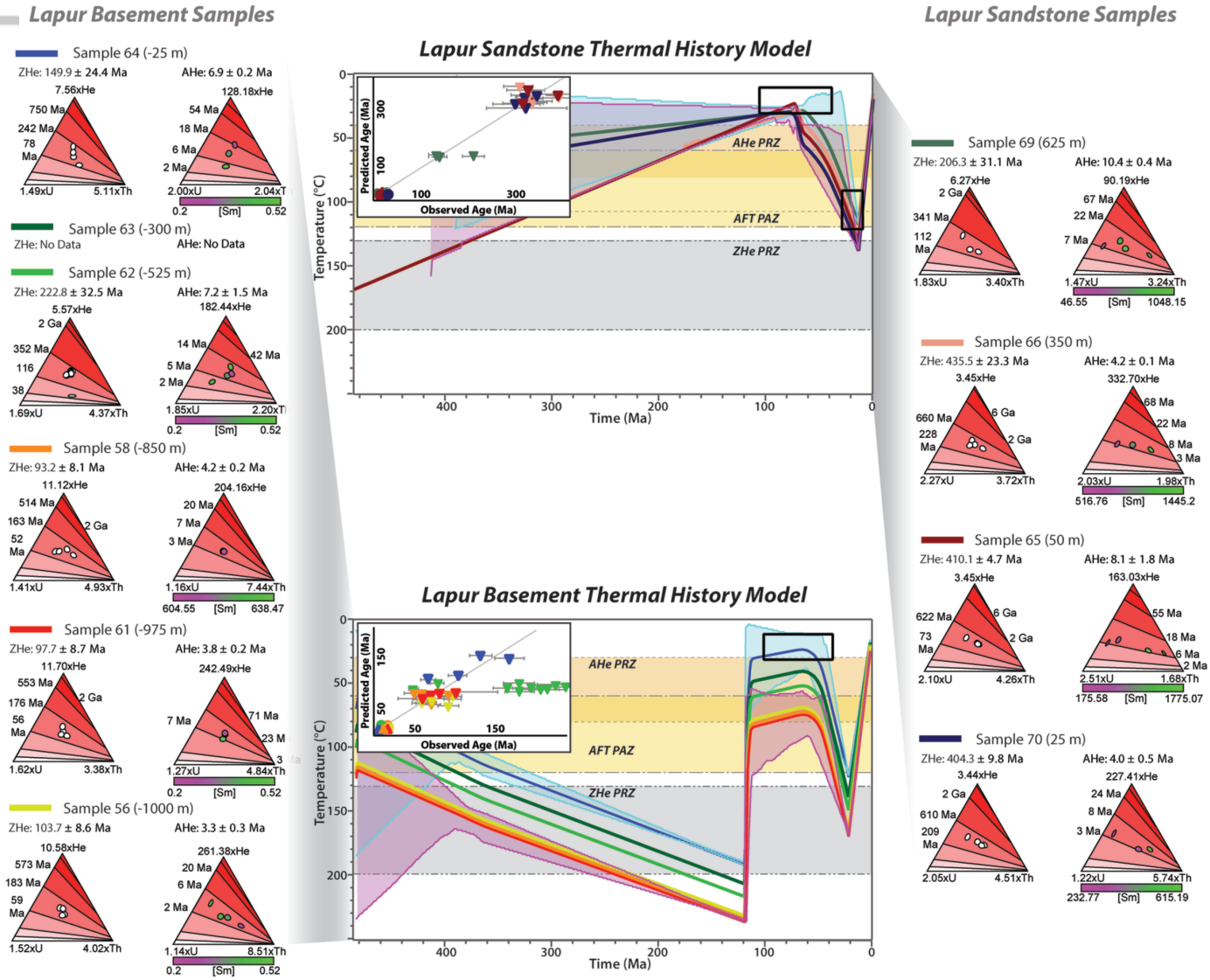

2017TC004575-f06-z-.tif

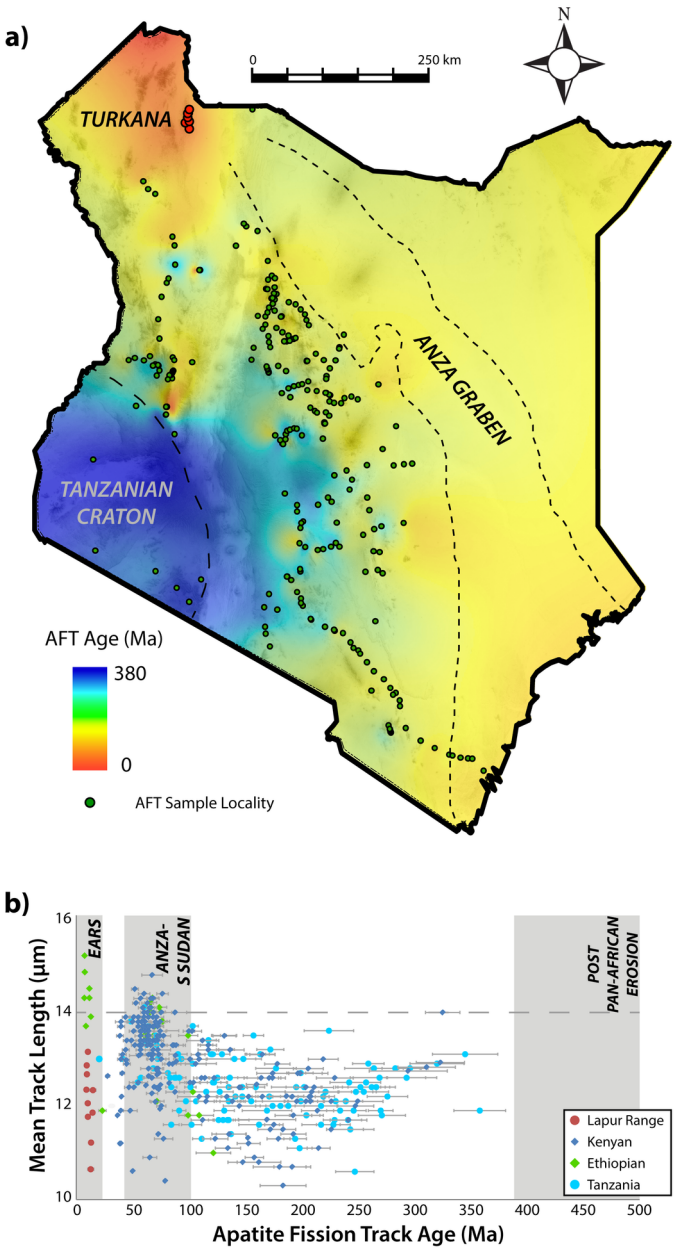

2017TC004575-f07-z-.tif

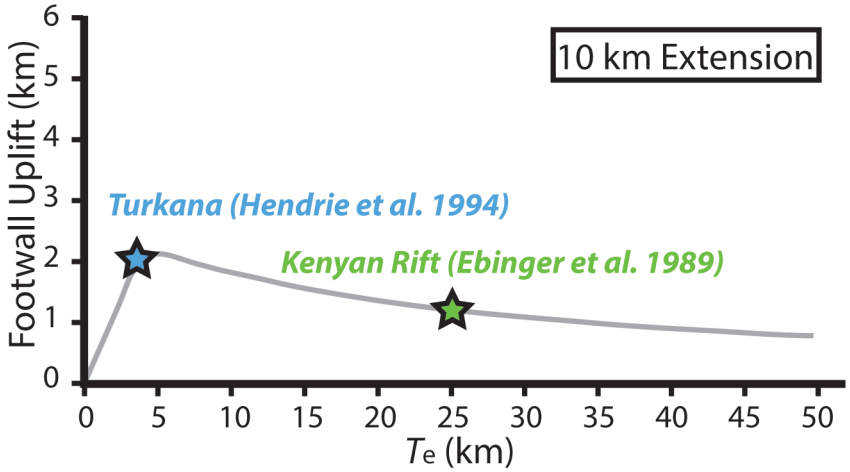

2017TC004575-f08-z-.tif